Heat Generation Effects on MHD Double Diffusive of Tio_2-Cu/Water Hybrid Nanofluids in a Lid-Driven Wavy Porous Cavity Using LTNE Condition

Mohammed A. Mansour[1], Sameh E. Ahmed[2], Eman F. Mohamed[3], Ahmed M. Ismaeel[1,4,*]
[1] Department of Mathematics, Faculty of Science, Assiut University, Assiut 71515 , Egypt
[2] Department of Mathematics, Faculty of Science, South Valley University, Qena 83523 , Egypt
[3] Department of Mathematics, Faculty of Engineering, Sphinx University, New Assiut City P.O. Box:10, Egypt
[4]Faculty of Basic Sciences, King Salman International University, South Sinai 46612, Egypt
* Corresponding author. Tel.: (+20) 1017855791
Email: mansour201354@yahoo.com (M. Mansour), sameh.hassan@sci.svu.edu.eg (S. Ahmed), Eman.fm@science.au.edu.eg (E. Mohamed), a.ismaeel@aun.edu.eg(A. Ismaeel)

Abstract:

In this manuscript, we study heat generation effects on Magnetohydrodynamic mixed convection in hybrid nanofluid (Tio2-Cu/Water) in a wavy porous cavity with a lid-driven using (LTNE) condition. The impacts of the inclined magnetic field, internal heat generation, and the volume of the solid fraction on the flow and heat structures are investigated. The dominant equations and the conditions of the boundaries are converted for dimensionless equations. This equation is solved numerically using the SIMPLER algorithm based on the finite volume method. The results are represented graphically by streamlines, isotherms, iso-concentrations, local Nusselt numbers, local Sherwood numbers, and average Nusselt numbers. The results showed that the isothermal wavy walls and the internal heat source had an essential effect on the fluid flow and heat transfer. Furthermore, the position of the heat source and large values of the heat generation parameter enhanced the rate of heat transfer and decreased the local Nusselt and Sherwood numbers. On the other hand, the rise of the Hartmann number restricted nanofluid transport. Moreover, the presence of a porous medium reduced the nanofluid velocity while enhancing the heat transport in the cavity.

Keywords: MHD, Double diffusion, heat generation/absorption, *Tio_2-Cu* nanoparticles, wavy cavity, thermal non-equilibrium condition.

Abbreviations

LTNE	Local thermal non-equilibrium
SIMPLE	Semi-implicit method for pressure linked equation
MHD	Magnetohydrodynamic
CFD	Computational Fluid Dynamics
(NPs)	nanoparticles

Nomenclature

b	heat source length
B	Dimensionless heat source length.
D	Position of a heat source.
p	Fluid pressure.
P	Dimensionless pressure.
q	Constant heat flux.
T	Temperature.
u,v	Velocity components in *x, y* directions.
U,V	Dimensionless velocity components
x, y	Cartesian coordinates.
X,Y	Dimensionless coordinates
B_0	Magnetic field strength.
H^*	Inter-phase heat transfer coefficient
Da	Darcy number.
Ha	Hartmann number·
Pr	Prandtl number.
Ri	Richardson parameter.
Re	Reynolds number
q	Constant heat flux.

Greek symbol

α	Thermal diffusivity (m^2s^{-1})
β	Coefficient of thermal expansion (K^{-1})
ε	Porosity of porous medium
θ	Dimensionless temperature
φ	Volume fraction nanoparticle
μ	Dynamic viscosity $(kg\ m^{-1}\ s^{-1})$
ν	Kinematic viscosity (m^2s^{-1})
ρ	Density $(kg\ m^{-3}\ )$
τ	Dimensionless time
σ	Electrical conductivity $(\Omega \cdot m)$

Subscripts

c	Cold
h	Hot
m	Average.
hnf	Hybrid nanofluid.
p	Nanoparticle.
f	Pure fluid.
s	Porous.

Q_0 Heat generation/absorption coefficient.

Sc Schemit number

Sh Schorword number.

1. INTRODUCTION

Heat and mass transport in a cavity with moving wavy walls have drawn the attention of many researchers due to their vast applications in medicine and engineering [1]–[3]. For instance, fluid flow in the esophagus digested food in the stomach and intestine, and blood flow in capillaries experience deformations for their external walls [4], [5]. There are different (CFD) techniques in the literature that are capable of mimicking the fluid, mass, and heat transport in the digestive organs in mammals [6], [7]. Nanotechnology provides promising applications in medicine [8]. In particular, (NPs) have been used as drug carriers [9], [10] in targeted therapy [11,12], tumor imaging agents [10], [13], [14] and internal heat source in the deep tissue [12], in the presence of external magnetic/electromagnetic radiation [15]. The suspended NPs in a fluid provides a new fluid with enhanced thermal properties, known as nanofluid [16]. In the case of suspending two different NPs in a fluid, the resulting fluid is known as a hybrid nanofluid [17]. The extinction physical and optical properties of both nanofluid and hybrid nanofluids drew the attention of many researchers in the past two decades [18]–[20]. The number of published articles investigating nanofluid increased from *648* articles in *2013* to *2425* articles in *2017*, according to the statistics of the web of science between *2013-2017* [21]. Most of these research articles were written by researchers in Iran, followed by researchers in India and Malaysia [21]. However, further studies are needed to address the long-term stability of NPs in the host fluid, the optimal cost of NP synthesis and the nanofluid/hybrid nanofluid preparation, and the optimal types of NPs used in the biological medium [22-24]. The majority of published work in nanofluid was about investigating mass and heat transfer in an enclosure (internal flow) or around it (external flow) [20], [25], which have vast applications in medicine and engineering. For instance, Nguyen et al. [19] studied the

influence of different shapes of *CuO* NPs on heat transfer in nanofluid flow within a wavy channel in the presence of obstacles. They also discussed the significance of the channel wavelength and height ratio in addition to the nanofluid velocity inlet. They used the numerical outputs to develop a correlation for Nusselt number as a function of Reynolds number and channel wall wavelength. They concluded that the heat transfer is proportional to the size of the obstacles. They also found that the spherical NPs increased the heat transfer by *55 %* compared to the other NP shapes. Uddin et al. [26] studied the heat transfer in a square vessel with a wavy surface filled in a nanofluid exposed to a magnetic field. They considered a nanofluid composed of Copper Oxide NPs suspended in water. They found that the magnetic field significantly impacted the fluid flow. The heat transfer decreased in the case of small NP sizes and Hartmann numbers. Interestingly, the heat transfer increased by *20 %* for the case of a wavy surface compared to the flat surface. Elshehabey et al. [20] investigated the flow of ferrofluid into a cavity through a hole at its wall. They used a non-linear Boussinesq approximation for the natural convection term. They found that the non-linear Boussinesq parameter significantly affected the fluid flow and entropy generation. Sheikholeslami and Oztop studied the impact of applying an external magnetic field source on Ferro-Nano fluid in an enclosure with a sinusoidal boundary. They found that bouncy forces enhanced the heat transport in the region adjacent to the hot wall. However, Lorentz's forces reduced the heat transfer in the enclosure. Cho [27] studied the natural convection of nanofluid in a cavity with wavy walls. He found that large values of the amplitude of the wavy surface and the nanoparticle volume fraction enhanced the heat transfer in the enclosure. Misirlioglu et al. [28] developed a mathematical model for nanofluid flow in a cavity with two wavy walls. They used Galerkin Finite Element Method to produce their outputs. They concluded that large values of the Rayleigh number resisted heat transfer across the hot wall where the Nusselt number had negative values. Sheremet et al. [29] considered the problem of nanofluid flow in an inclined wavy enclosure with an isothermal corner heater. They developed a single-phase nanofluid model to investigate the heat transfer in the cavity. They found that the Hartmann number reduced the advection flow and heat transfer rates. They also found that in

the case of an acute angle of the magnetic field, the convective flow was enhanced due to the reduction of the buoyancy force. They concluded that increasing NP volume fraction improved the fluid flow and the heat transfer in the cavity. Ahmed and Rashed [30] provided a numerical simulation of magnetohydrodynamic flow and heat transfer inside a cavity with one wavy side. They considered the flow through a porous medium in the presence of a heat source across the whole cavity, which was exposed to a magnetic field. They found that the heat transfer was enhanced by increasing the undulation number, the wavy contraction ratio, and the Hartmann number. They also found that increasing the heat generation parameter reduced the thermal boundary later thickness near the wavy wall. Abdulkadhim et al. [31] developed a mathematical model to investigate the heat and mass transport in a wavy cavity that comprises a hot cylinder at its centre. They considered the case when the cavity was exposed to a magnetic field. They reported that the Hartmann number had an insignificant impact on the computed Nusselt number. They investigated the effect of heat generation and heat sink in the cavity. They found that the Nusselt number value increased by a third in the heat sink case while reducing by half in the case of the heat source. However, this impact was noticed for low values of the Rayleigh number. Ahmed [32] used fractional differential equations to study heat transfer by natural advection in a horizontal channel with wavy walls. He found that the increase in surface deformation parameters enhanced the heat and mass in the channel. Mansour and Bakier [1] considered heat transfer in a cavity with complex wavy walls. They investigated the influence of NP volume fraction on Nusselt and Rayleigh numbers which increased with increasing the NP volume fraction. Rashed et al. [2] studied nanofluid for hybrid flow in the inclined enclosure with two-sides wavy. They investigated the influence of magnetic fields and heat transfer by radiation. They found that increasing the radiation rate enhanced the heat transfer.

In this manuscript, we consider the problem of heat and mass transfer in Tio_2-Cu/Water hybrid nanofluid in a cavity with one wavy side using a local non-equilibrium thermal condition. We investigate the case when the

cavity is exposed to an inclined magnetic field that interacts with the nanoparticles creating internal heat generation.

2. Mathematical modelling

We consider heat and mass transport in a cavity with one wavy side filled in a hybrid nanofluid, as shown in Fig. 1. We consider the cavity interior space comprised of a porous medium. We also consider a vertical segment of heat source, with length *b*, at the cavity left wall, while the other vertical wall is adiabatic. The right side wall is cold (T_c), the bottom and top walls are adiabatic and have lid velocities. The convection of mongrel nanofluid is not in thermodynamic local equilibrium conditions. The magnetic field direction has an inclination Φ. Dirichlet type boundary conditions are applied at all cavity boundaries. The previously hypotheses have been written in the following equations: (1:6) for the hybrid nanofluid flow, which is a steady-state flow, incompressible, single-phase, laminar ([27], [33])

$$\frac{\partial u}{\partial x}+\frac{\partial v}{\partial y}=0 \tag{1}$$

$$\frac{1}{\varepsilon^2}\left(u\frac{\partial u}{\partial x}+v\frac{\partial u}{\partial y}\right)=-\frac{1}{\rho_{hnf}}\frac{\partial p}{\partial x}+\frac{1}{\varepsilon}.\nu_{hnf}.\nabla^2 u-\frac{\nu_{hnf}}{K}.u+\frac{\sigma_{hnf}B_0^2}{\rho_{hnf}}\left(v\sin\Phi\cos\Phi-u\sin^2\Phi\right) \tag{2}$$

$$\begin{aligned}\frac{1}{\varepsilon^2}\left(u\frac{\partial v}{\partial x}+v\frac{\partial v}{\partial y}\right)=&-\frac{1}{\rho_{hnf}}\frac{\partial p}{\partial y}+\frac{\nu_{hnf}}{\varepsilon}.\nabla^2\,\mathrm{v}-\frac{\nu_{hnf}}{K}v+\frac{\sigma_{hnf}B_0^2}{\rho_{nf}}\left(u\sin\Phi\cos\Phi-v\cos^2\Phi\right)\\&+\frac{(\rho\beta)_{hnf}}{\rho_{hnf}}g(T_f-T_c)+\frac{(\rho\beta^*)}{\rho_{hnf}}g(\mathrm{C}-\mathrm{C}_c)\end{aligned} \tag{3}$$

$$\frac{1}{\varepsilon}\left(u\frac{\partial T_f}{\partial x}+v\frac{\partial T_f}{\partial y}\right)=\alpha_{eff.hnf}.\nabla^2 T_f+\frac{h_{hnfs}(T_s-T_f)}{\varepsilon(\rho\,\mathrm{c}_p)_{hnf}}+\frac{Q_0}{\varepsilon(\rho\,\mathrm{c}_p)_{hnf}} \tag{4}$$

$$0=(1-\varepsilon).\mathrm{k}_s.\nabla^2\,\mathrm{T}_s+h_{hnfs}(T_f-T_s)+(1-\varepsilon)\,\mathrm{Q}_0 \tag{5}$$

$$u\frac{\partial C}{\partial x}+v\frac{\partial C}{\partial y}=D_B.\nabla^2 C \tag{6}$$

The flow field required boundary conditions are taken as

On the bottom:

$$u = \pm\lambda_d U_0, v = 0, \quad 0 \le x \le H,$$
$$\frac{\partial T_f}{\partial y} = \frac{\partial T_s}{\partial y} = \frac{\partial C}{\partial y} = 0 \tag{7}$$

On the top:

$$u = \pm\lambda_t U_0, v = 0, \quad 0 \le x \le H,$$
$$\frac{\partial T_f}{\partial y} = \frac{\partial T_s}{\partial y} = \frac{\partial C}{\partial y} = 0 \tag{8}$$

On the left

$$u = v = 0,\ 0 \le x \le H$$
$$\frac{\partial T_f}{\partial x} = -\frac{q_w}{k_{hnf}}, \frac{\partial T_s}{\partial x} = -\frac{q_w}{k_s}, \frac{\partial C}{\partial x} = -\frac{q_w^*}{D_m}, \tag{9}$$
$$d - 0.5b \le y \le d + 0.5b, \quad \frac{\partial T_f}{\partial x} = \frac{\partial T_s}{\partial x} = \frac{\partial C}{\partial x} = 0 \ \textit{othrwise}$$

On the right:

$$u = v = 0, \mathrm{T}_f = T_s = \mathrm{T}_c, \mathrm{C} = \mathrm{C}_c, x = H - AH\left[1 - \cos\left(2\pi\lambda y / \mathrm{H}\right)\right] \tag{10}$$

where v, T, C, ρ_{hnf}, ν_{hnf} , g, p , μ_{hnf} and Q_0 are the fluid velocity components, temperature, concentration, density, kinematic viscosity, gravity, pressure, dynamic viscosity, and heat generation, respectively.

The dimensionless set is introduced in Eq. (11):

$$X=\frac{x}{H},\ Y=\frac{y}{H},\ U=\frac{u}{U_0},\ V=\frac{v}{U_0},\ P=\frac{p}{\rho_{nf}U_0^2},\ \theta_f=\frac{(T_f-T_c)}{q_w H}.k_f,$$
$$\theta_s=\frac{(T_s-T_c)}{q_w H}.k_s,\ \varphi=\frac{(\mathrm{C}-C_c)}{q_w^{*}H}.\mathrm{D}_m,\ Ri=\frac{Gr}{\mathrm{Re}^2},\ \mathrm{Re}=\frac{U_0 H}{\nu_f},\ \mathrm{D}=\mathrm{d}/\mathrm{H},\ \mathrm{B}=\mathrm{b}/\mathrm{H} \tag{11}$$

By applying these transformations to Eqs. (1)- (6) produced the following dimensionless equations:

$$\frac{\partial U}{\partial X}+\frac{\partial V}{\partial Y}=0, \tag{12}$$

$$\frac{1}{\varepsilon^2}\left(U\frac{\partial U}{\partial X}+V\frac{\partial U}{\partial Y}\right)=-\frac{\partial P}{\partial X}+\frac{1}{\varepsilon.\mathrm{Re}}.\left(\frac{\rho_f}{\rho_{hnf}}\right)\left(\frac{\mu_{hnf}}{\mu_f}\right).\nabla^2\,\mathrm{U}-\frac{1}{Da.\mathrm{Re}}.\left(\frac{\rho_f}{\rho_{hnf}}\right)\left(\frac{\mu_{hnf}}{\mu_f}\right).U$$
$$+\left(\frac{\rho_f}{\rho_{hnf}}\right)\left(\frac{\sigma_{hnf}}{\sigma_f}\right).\frac{Ha^2}{\mathrm{Re}}\left(V\sin\Phi\cos\Phi-U\sin^2\Phi\right) \tag{13}$$

$$\frac{1}{\varepsilon^2}\left(U\frac{\partial V}{\partial X}+V\frac{\partial V}{\partial Y}\right)=-\frac{\partial P}{\partial Y}+\frac{1}{\varepsilon.\mathrm{Re}}.\left(\frac{\rho_f}{\rho_{hnf}}\right)\left(\frac{\mu_{hnf}}{\mu_f}\right).\nabla^2\,\mathrm{V}-\frac{1}{Da.\mathrm{Re}}.\left(\frac{\rho_f}{\rho_{hnf}}\right)\left(\frac{\mu_{hnf}}{\mu_f}\right).\mathrm{V}$$
$$+Ri.\frac{(\rho\beta)_{hnf}}{\rho_{hnf}.\beta_f}.\theta_f+Gr_c.\phi+\left(\frac{\rho_f}{\rho_{hnf}}\right)\left(\frac{\sigma_{hnf}}{\sigma_f}\right)\frac{Ha^2}{\mathrm{Re}}\left(U\sin\Phi\cos\Phi-V\cos^2\Phi\right) \tag{14}$$

$$\frac{1}{\varepsilon}\left(U\frac{\partial\theta_f}{\partial X}+V\frac{\partial\theta_f}{\partial Y}\right)=\left(\frac{1}{\mathrm{Re}.\mathrm{Pr}}\right)\frac{\alpha_{eff.\mathrm{h}nf}}{\alpha_f}.\nabla^2\theta_f+\frac{1}{\varepsilon.\mathrm{Re}.\mathrm{Pr}}\frac{(\rho c_p)_f}{(\rho c_p)_{hnf}}.\mathrm{H}^{*}(\theta_s-\theta_f)$$
$$+\frac{1}{\varepsilon.\mathrm{Re}.\mathrm{Pr}}\frac{(\rho c_p)_f}{(\rho c_p)_{hnf}}.\mathrm{Q} \tag{15}$$

$$U\frac{\partial\varphi}{\partial X}+V\frac{\partial\varphi}{\partial Y}=\frac{1}{\mathrm{Re}.Sc}\left(\frac{\partial^2\varphi}{\partial X^2}+\frac{\partial^2\varphi}{\partial Y^2}\right) \tag{16}$$

where

$$\mathrm{Pr}=\frac{\nu_f}{\alpha_f},\ Gr=\frac{g\beta_f H^4 q_w}{\nu^2{}_f.k_f},\ \mathrm{Ha}=B_0 H\sqrt{\sigma_f/\mu_f},$$
$$Da=\frac{K}{H^2},\ H^{*}=h_{hnfs}.\frac{H^2}{k_f},\ \mathrm{k}_{fs}=\frac{k_f}{k_s},\ K_r=\frac{k_f}{(1-\varepsilon)\,\mathrm{k}_s}, \tag{17}$$

The corresponding boundary conditions (7-10) become:

The wall left

$$U = V = 0, \quad 0 \le Y \le 1,$$
$$\frac{\partial \theta_f}{\partial X} = -\frac{k_f}{k_{nf}}, \frac{\partial \theta_s}{\partial X} = -1, \frac{\partial \varphi}{\partial X} = -1, \tag{19}$$
$$D - 0.5B \le Y \le D + 0.5B, \quad \frac{\partial \theta_f}{\partial X} = \frac{\partial \theta_s}{\partial X} = \frac{\partial \varphi}{\partial X} = 0 \ \textit{othrwise}$$

The wall right

$$\mathrm{U} = V = 0, \theta_f = \theta_s = \varphi = 0 : \ X = 1 - A\left[1 - \cos\left(2\pi\lambda Y\right)\right], 0 \le Y \le 1 \tag{20}$$

The wall bottom:

$$U = \pm\lambda_d, V = 0, \frac{\partial \theta_f}{\partial Y} = \frac{\partial \theta_s}{\partial Y} = \frac{\partial \varphi}{\partial Y} = 0 \quad , 0 \le X \le 1 \tag{21}$$

The top wall

$$U = \pm\lambda_t, V = 0, \frac{\partial \theta_f}{\partial Y} = \frac{\partial \theta_s}{\partial Y} = \frac{\partial \varphi}{\partial Y} = 0 \quad , 0 \le X \le 1 \tag{22}$$

The Nu_s of fluid and solid are defined as:

$$Nu_{fs} = \left[\frac{1}{(\theta_f)_{hot}}\right]_{X=0}, Nu_{ss} = \left[\frac{1}{(\theta_s)_{hot}}\right]_{X=0} \tag{23}$$

The local Schorword number is defined as:

$$Nu_{mf} = \frac{1}{B}\int_{D-0.5B}^{D+0.6B} Nu_{fs}\, dY, Nu_{ms} = \frac{1}{B}\int_{D-0.5B}^{D+0.6B} Nu_{ss}\, dY, \tag{24}$$

Also, the Nu_m of fluid and solid are defined as:

$$Nu_{mf} = \frac{1}{B}\int_{D-0.5B}^{D+0.6B} Nu_{fs}\, dY \;, Nu_{ms} = \frac{1}{B}\int_{D-0.5B}^{D+0.6B} Nu_{ss}\, dY \;, \tag{25}$$

The average Schorword number is defined as:

$$Sh = \frac{1}{B}\int_{D-0.5B}^{D+0.6B} Sh_s\, dY \tag{26}$$

In Eqs. (12) - (17), $\alpha_{eff,hnf}$ and $\alpha_{eff,f}$ are equal to:

$$\alpha_{eff,hnf} = \frac{k_{eff,hnf}}{\left(\rho c_p\right)_{hnf}} \tag{27}$$

$$\alpha_{eff,f} = \frac{k_{eff,f}}{\left(\rho c_p\right)_{f}} \tag{28}$$

where

$$k_{eff,hnf} = \varepsilon k_{hnf} + \left(1-\varepsilon\right)k_s \tag{29}$$

$$k_{eff,f} = \varepsilon k_{f} + \left(1-\varepsilon\right)k_s \tag{30}$$

The mathematical expressions of μ_{hnf}, k_{hnf}, $\left(c_p\right)_{hnf}$, β_{hnf}, σ_{hnf} and ρ_{hnf} are as follows:

$$\frac{\alpha_{hnf}}{\alpha_f} = \frac{k_{hnf}/k_f}{(\rho c_p)_{hnf}/(\rho c_p)_f} \tag{31}$$

$$\frac{\rho_{hnf}}{\rho_f}=\left(1-\phi_{Cu}\right)\left(1-\phi_{TiO_2}+\phi_{TiO_2}\frac{\rho_{TiO_2}}{\rho_f}\right)+\phi_{Cu}\frac{\rho_{Cu}}{\rho_f} \tag{32}$$

$$\frac{\left(\rho C_p\right)_{hnf}}{\left(\rho C_p\right)_f}=\left(1-\phi_{Cu}\right)\left(1-\phi_{TiO_2}+\phi_{TiO_2}\frac{\left(\rho C_p\right)_{TiO_2}}{\left(\rho C_p\right)_f}\right)+\phi_{Cu}\frac{\left(\rho C_p\right)_{Cu}}{\left(\rho C_p\right)_f} \tag{33}$$

$$\frac{\beta_{hnf}}{\beta_f}=\left(1-\phi_{Cu}\right)\left(1-\phi_{TiO_2}+\phi_{TiO_2}\frac{\beta_{TiO_2}}{\beta_f}\right)+\phi_{Cu}\frac{\beta_{Cu}}{\beta_f} \tag{34}$$

$$\frac{k_{hnf}}{k_{bf}}=\frac{k_{Cu}+2k_{bf}-2\phi_{Cu}\left(k_{bf}-k_{Cu}\right)}{k_{Cu}+2k_{bf}+\phi_{Cu}\left(k_{bf}-k_{Cu}\right)} \tag{35}$$

Where $\frac{k_{bf}}{k_f}=\frac{k_{TiO_2}+2k_f-2\phi_1\left(k_f+k_{TiO_2}\right)}{k_{TiO_2}+2k_f+\phi_1\left(k_f-k_{TiO_2}\right)}$ (36)

$$\frac{\sigma_{hnf}}{\sigma_{bf}}=\frac{\sigma_{Cu}+2\sigma_{bf}-2\phi_{Cu}\left(\sigma_{bf}-\sigma_{Cu}\right)}{\sigma_{Cu}+2\sigma_{bf}+\phi_{Cu}\left(\sigma_{bf}-\sigma_{Cu}\right)} \tag{37}$$

Where $\frac{\sigma_{bf}}{\sigma_f}=\frac{\sigma_{TiO_2+}2\sigma_f-2\phi_{TiO_2}\left(\sigma_f-\sigma_{TiO_2}\right)}{\sigma_{TiO_2+}2\sigma_f+\phi_{TiO_2}\left(\sigma_f-\sigma_{TiO_2}\right)}$ (38)

The previous equations (31-38) presented the mathematical expressions for thermal diffusivity, effective density, heat capacitance, thermal expansion, thermal conductivity, and the hybrid nanofluid's effective dynamic viscosity, respectively. The thermo-physical properties value of H_2O, Cu and TiO_2 are given in Table 1.

1. Numerical solution and Validation

We solve the system of dimensionless equations (12-17) along with the dimensionless boundary conditions (18-22) using the finite volume method. Furthermore, the finite volume method [35], [36] is extended to the non-orthogonal grids. This technique starts with the following grid transformation:

$$\eta = Y,\ \xi = \frac{X}{1 - A(1 - \cos(2\pi\lambda Y)} \tag{39}$$

In Fig. 2, the transformation between the asymmetrical domain and calculation domain is illustrated. In the same context, the convective terms in the case of the non-orthogonal grids are expressed as:

$$\frac{\partial(U\vartheta)}{\partial X} + \frac{\partial(V\vartheta)}{\partial X} = \frac{1}{J^*}\left[\frac{\partial}{\partial\xi}(U^*\vartheta) + \frac{\partial}{\partial\eta}(V^*\vartheta)\right] \tag{40}$$

where

$$J^* = X_\xi Y_\eta - X_\eta Y_\xi,\ U^* = \chi_{11}U + \chi_{21}V,\ V^* = \chi_{22}V + \chi_{12}U \tag{41}$$

$$\chi_{11} = Y_\eta, \chi_{12} = -Y_\xi, \chi_{21} = -X_\eta, \chi_{22} = X_\xi \tag{42}$$

Furthermore, the viscous terms are given by:

$$\frac{\partial}{\partial X}\left[\frac{\partial\vartheta}{\partial X}\right] + \frac{\partial}{\partial Y}\left[\frac{\partial\vartheta}{\partial Y}\right] = \frac{1}{J^*}\frac{\partial}{\partial\xi}\left[\alpha_{11}\frac{\partial\vartheta}{\partial\xi} + \alpha_{12}\frac{\partial\vartheta}{\partial\eta}\right] + \frac{1}{J^*}\frac{\partial}{\partial\eta}\left[\alpha_{22}\frac{\partial\vartheta}{\partial\eta} + \alpha_{12}\frac{\partial\vartheta}{\partial\xi}\right],\tag{43}$$

where

$$\alpha_{11} = \frac{\alpha^*}{J^*} = \frac{X_\eta^2 + Y_\eta^2}{J^*}, \qquad \alpha_{22} = \frac{\gamma^*}{J^*} = \frac{X_\xi^2 + Y_\xi^2}{J^*} \tag{44}$$

Where J^* is the Jacobi factor, α^*, γ^* are metric coefficients in the x and h-directions in the computational plane. Here, the second upwind scheme is applied to evaluate the advection terms. In contrast, the central difference schemes are used to process the Laplace operators in the previous system, and the alternating direction implicit is used to solve the algebraic system obtained. The approximate standard is considered 10^{-6}. Also, the most suitable grid for all computations was found of size101×101. Fig. 3 reveals

comparisons between the present simulation outputs the results obtained by Cheong et al. [35] in the case (f=Ha=Q=0) showing excellent agreement.

4. Discussion:

We introduce the results of our model in terms of the key model parameters such as the size of the heat source (*B*), which is changes from 0.2 to 0.8, the position of the heat generation (*D*), which varies from 0.3 to 0.7, the generation parameter (*Q*) of heat which is varied from (0 to 2), the effects of Hartmann number (*Ha*) which is diverse between (0 to 100), the undulation parameter (λ) which is varied from 1 to 5, the coefficient of inter-phase heat transfer (H^*) which is varied from 0 to 10, the Darcy parameter (Da) which changes from 10^{-1} to 10^{-5}, the magnetic field inclination angle (Φ) which is between $0^0 - 90^0$ and the solid volume fraction (ϕ_{Cu}) at the values 0, $\frac{\phi}{2}$ and ϕ. The obtained results have been illustrated using streamlines, iso concentrations, fluid phase and solid phase of isotherm, local and average Nusselt number, and Sherwood numbers. The values for the baseline parameters are given by:

$$Ha = 10, \phi = 0.05, Q = 1, \mathrm{B} = 0.5, D = 0.5, \lambda = 2, \Phi = \pi / 2, Da = 10^{-3}, \phi_{Cu} = \phi_{TiO_2} = \phi / 2, K_{r=1}, \lambda_d = \lambda_t = 1$$

Impact of the size of the source of heat (B):

Fig. 4 displays the streamlines contours, isotherms of the fluid and nanoparticles, and iso-concentrations for different values of *B*. **Fig. 4 (a)** shows that when increasing the size B from 0.2 to 0.8, there is no significant impact on the streamlines. On the other hand, **Fig. 4 (b)** depicts enhancement in heat transfer in the fluid due to the increase in the length of the heat source *B*. As shown in **Fig. 4 (c)**, the large size of the heat source makes the isotherms primarily horizontal, and their gradients become vertically extended along the cavity. **In Fig. 4 (d),** iso-concentration is expanded across the cavity as the heat source length B increases. **Figs. 5 (a,b)**

is pictorial of Nu for the fluid phase Nu_{fs} and the solid phase Nu_{ss}. It is noticeable that the heat distribution is symmetrical around the heat source position.

Effect of heat generation position (D):

Fig. 6 (a-d) show the contours of Ψ, T of the two-phase fluid, and iso-concentrations for diverse values of the position D for heat source when the hybrid nanofluid volume fraction is at $\phi_{Cu} = \phi_{TiO_2} = \phi / 2$, $\phi = 0.05$,

There is no influence on the streamlines contours when D is changing from the bottom ($D = 0.3$) to the upper ($D = 0.7$) part of the left side of the cavity, see **Fig. 6 (a)**. However, **Fig. 6 (b)** and **(c)** show isotherms of the two phases, which vary in density according to D. **Fig. 6 (d)** shows that iso-concentrations are also significantly influenced by the heat source location. **Fig. 7 (a)** and **(b)** present the impacts of D on the Nu for the fluid phase Nu_{fs} and the solid phaseNu_{ss}.

Effects of the Parameter (Q):

Fig. 8 introduces Ψ, T_f, T_sAnd iso-concentrations according to the variation in the heat generation coefficient Q. **In Fig. 8 (b-c)**, an increase in Q elevates the fluid and stable temperatures in the cavity.

In Fig. 8 (a-d), There are minor effects on the contours of the streamlines and iso-concentrations due to the increase in heat generation coefficient Q. **Fig. 9 (a-b)** show the impacts of Q on the Nu_{fs}, and Nu_{ss} Along with the heat source. It was found that there is an asymmetry in the distribution of both the Nu_{fs}, and the Nu_{ss} across the cavity, in addition, the increase in Q declines Nu_{fs} and Nu_{ss}.

Impact of Hartman number (Ha):

In **Fig. 10 (a),** we show the Hartmann number effect (Ha) on the streamlines distribution. The flow pattern in the cavity is affected strongly by the field of magnetic, which controls the flow pattern inside the cavity. The fluid moves clockwise into the center of the cavity because of the exposure to the magnetic field. **In Fig. 10 (b-d),** the isotherms are enhanced due to the increase in Ha. On the other hand, large Hartman values make

the isotherms distribute in parallel curves, see **Fig. 10 (c)**, because of the restricting of the Lorentz force for the fluid motion. The Lorentz force increases as the Ha increases. Furthermore, the increase in the Hartman number reduces Nu_{fs} and u_{ss} , see **Fig. 11 (a-b),** which means that the Lorentz force obstructs the convection in both phases.

Effects of the Undulation Parameter (λ):

Fig. 12 (a) demonstrates the impact of the undulation parameter on the fluid. An increase in λ tends to condense the main convective flow inside the cavity. The improvement in the waviness of the hot wall indicates an essential modification in the vorticity of the streamlines. The significant influence of the undulation parameter on the distribution of streamliners is due to changes in geometry. The isotherms of two phases for various numbers of undulation parameters are shown in **Fig. 12 (b-d).** The temperature contours reflect the influence of the distribution of the temperature sinusoidal in the cavity. When changing the value of $\lambda = 1,3$ and 5, the distribution of T acts like the wave shape of the right wall, where along the wavy wall, the thermal boundary layer is formed. The increase in λ increases the difficulty of the flow domain and thus decreases transport convective. **Fig. 13 (a-b)** illustrates the variation of N_u at the sidewalls for various values of the λ. The variation of N_u for fluid and solid decreases as λ increases.

Effects of the inter-phase heat transfer coefficient (H^*):

Fig. 14 (a) presents the local values of Nu_{fs} which decrease with the increase in the value of H^*. Besides, Nu_{mf} along ϕ for different values of H^* has been shown in **Fig. 15**. In this figure, the large values of H^* reduce Nu_{ms}. Further, the increase of ϕ enhances Nu_{mf}. Furthermore, **Fig. 16 (a-b) s**hows that N_{uf} and N_{us} decreases as ϕ_{Cu} increases.

Effects of the Darcy parameter (Da):

The influence of a Darcy parameter on Ψ and T have been shown in **Fig. 17 (a-d).** In **Fig 17 (a),** the reduction in Da restricts the fluid flow because of the increase in the resistance of the porous medium. As a result, when Da has a value in the range between 10^{-5} and 10^{-1}, the absolute fluid velocity is reduced by 90.91%, see **Fig. 17 (b-d)**. Thus, a reduction of Da is attractive Ψ of the two phases within a wavy cavity. In **Fig. 18 (a-b),** a descend in Da decreases the values of Nu for the two phases.

Effect of the magnetic field inclination angle (Φ)

In Figs. 19 (a-b), the outlines of Nu at the heated segment are illustrated for different inclination angle values when Ha=10 and B=0.5. The results disclosed a significant reduction in values of Nu when the inclination angle is increasing, which can be explained as when the inclination angle is increased, the Lorentz force is enhanced, which in turn reduces the heat transfer by convection.

Conclusion:

This paper presents the problem of hybrid nanofluids for mixed convection inside an undulating porous cavity. First, the contours of Ψ and T are discussed for fluid/solid phases and iso-concentrations. Then, also, introduced Nu and Nu_m of two phases, as well as the local Schorword number beneath the differences of the critical parameters like length of heat source (B), coefficient of heat generation/absorption (Q), the position of heat source (D), Hartmann number (Ha), porosity parameter (ε), coefficient of an inter-phase heat transfer (H^*), undulation parameter (λ), Darcy parameter (Da), magnetic field inclination angle (Φ), and Solid volume fraction (ϕ_{Cu}).

The most important points can be summarized as follows:

- The partial heat source length and position are significantly affected in setting the properties of nanofluid movements and heat transfer inside the cavity.
- Increasing the values of Ha from 0 to 50 reduces the maximum of the streamlines and reduces Nu_{fs}, Nu_{mf} and Nu_{ms}. Physically, the increase in Ha enhances the magnetic Lorentz force.

- The different values of H^* affect significantly Ψ_s porfile.
- The increasing of the nanoparticle concentration enhances the values of Nu_{mf}.
- Ψ_f and Ψ_s within the cavity are enhanced when the nanofluid movements are reduced due to the increase in resistance of a porous medium.

Acknowledgements

The authors thanks Prof. Mansour for helping with the problem modelling and the numerical simulation.

Funding

Not applicable.

Availability of data and materials

Not applicable.

Competing interests

The authors declare that they have no competing interests.

Authors' contributions

Prof. Mohamed developed and solved the problem, whereas Dr Ahmed wrote the introduction, reviewed the literature, and proofread the manuscript. In addition, Dr Sameh revised the manuscript and contributed to writing the discussion. Finally, Ms Eman wrote the paper. All authors reviewed the manuscript, read, and approved the submitted version.

References

[1] Mansour, M. A., and Bakier, M. A. "Free convection heat transfer in complex-wavy-wall enclosed cavity filled with nanofluid", *International communications in heat and mass transfer*, **44**, pp. 108–115 (2013).

[2] Rashed, Z. Z., Mansour, M. A., Attia, M. A., et al. "Numerical study of radiative impacts on a magneto-convective flow confined an inclined two-sided wavy enclosure using hybrid nanofluid", *Physica Scripta*, **96**(2), pp. 25216 (2020).

[3] Sheikholeslami, M., and Oztop, H. F. “MHD free convection of nanofluid in a cavity with sinusoidal walls by using CVFEM”, *Chinese Journal of Physics*, **55**(6), pp. 2291–2304 (2017).

[4] Jafari, A., Zamankhan, P., Mousavi, S. M., et al. “Numerical investigation of blood flow. Part II: In capillaries”, *Communications in Nonlinear Science and Numerical Simulation*, **14(4)**, pp. 1396–1402 (2009).

[5] Ibitoye, S. E., Adegun, I. K., Omoniyi, P. O., et al. “Numerical investigation of thermo-physical properties of the non-newtonian fluid in a modeled intestine”, *Journal of Bioresources and Bioproducts*, **5**(3), pp. 211–221 (2020).

[6] Kozu, H., Kobayashi, I., Neves. M. A., et al. “PIV and CFD studies on analyzing intragastric flow phenomena induced by peristalsis using a human gastric flow simulator,” *Food & function*, **5**(8), pp. 1839–1847 (2014).

[7] Ferrua, M. J., and Singh, R. P. “Modeling the fluid dynamics in a human stomach to gain insight of food digestion”, *Journal of food science*, **75**(7), pp. R151–R162 (2010).

[8] Klębowski, B., Depciuch, J., Parlińska-Wojtan, M., et al. “Applications of noble metal-based nanoparticles in medicine”, *International Journal of molecular sciences*, **19**(12), pp. 4031 (2018).

[9] Qin, Z., and Bischof, J. C. “Thermophysical and biological responses of gold nanoparticle laser heating”, *Chemical Society Reviews*, **41**(3), pp. 1191–1217 (2012).

[10] Jain, S.,Hirst, D., and O’Sullivan, J. “Gold nanoparticles as novel agents for cancer therapy,” *The British Journal of Radiology*, **85**(1010), pp. 101–113, 2014.

[11] Skinner, M. G., Iizuka, M. N., Kolios, M. C., et al. “A theoretical comparison of energy sources-microwave, ultrasound and laser-for interstitial thermal therapy”, *Physics in Medicine & Biology*, **43**(12), pp. 3535 (1998).

[12] Ismaeel, A. M. "A mathematical model for photothermal therapy of spherical tumors", PhD diss., University of Glasgow (2020).

[13] Arami, H., Khandhar, A., Liggitt, D., et al. “In vivo delivery, pharmacokinetics, biodistribution, and toxicity of iron oxide nanoparticles”, *Chemical Society Reviews*, **44**(23), pp. 8576–8607 (2015).

[14] Cherukuri, P., Glazer, E. S., and Curley, S. A. “Targeted hyperthermia using metal nanoparticles”, *Advanced Drug Delivery Reviews*, **62**(3), pp. 339–345 (2010).

[15] Kaur, P., Aliru, M. L., Chadha, A. S. A., et al. “Hyperthermia using nanoparticles–Promises and pitfalls”, *International Journal of Hyperthermia*, **32**(1), pp. 76–88 (2016).

[16] Buongiorno, J. “Convective transport in nanofluids”, **128**(3), pp. 240-250 (2006).

[17] Wang, X., Xu, X., and Choi, S. U. S. “Thermal conductivity of nanoparticle-fluid mixture”, *Journal of thermophysics and heat transfer*, **13**(4), pp. 474–480 (1999).

[18] Hady, F., Ibrahim, F., El-Hawary, H., et al. “Effect of Suction/Injection on Natural Convective Boundary-Layer Flow of A Nanofluid Past A Vertical Porous Plate Through A Porous Medium”, *Journal of Modern Methods in Numerical Mathematics*, **3**(1), pp. 53-63 (2012).

[19] Nguyen, T. K., Saidizad, A., Jafaryar, M., *et al.* “Influence of various shapes of CuO nanomaterial on nanofluid forced convection within a sinusoidal channel with obstacles”, *Chemical Engineering Research and Design*, **146**, pp. 478–485 (2019).

[20] Elshehabey, H. M., Raizah, Z., Öztop, H. F., et al. “MHD natural convective flow of Fe_3O_4− H_2O ferrofluids in an inclined partial open complex-wavy-walls ringed enclosures using non-linear Boussinesq approximation”, *International Journal of Mechanical Sciences*, **170**, pp. 105352 (2020).

[21] Babar, H., and Ali, H. M. “Towards hybrid nanofluids: preparation, thermophysical properties, applications, and challenges”, *Journal of Molecular Liquids*, **281**, pp. 598–633 (2019).

[22] Sarkar, J., Ghosh, P., and Adil, A. “A review on hybrid nanofluids: recent research, development, and applications”, *Renewable and Sustainable Energy Reviews*, **43**, pp. 164–177 (2015).

[23] Ismaeel, A. M., Mansour, M. A., Ibrahim, F. S., et al. "Numerical simulation for nanofluid extravasation from a vertical segment of a cylindrical vessel into the surrounding tissue at the microscale", *Applied Mathematics and Computation* **417**, pp. 126758 (2022).

[24] Ismaeel, A. M., Kamel, R. S., Hedar, M. R., et al. "Numerical simulation for a Casson nanofluid over an inclined vessel surrounded by hot tissue at the microscale", *SN Applied Sciences*, **5**(8), pp. 223 (2023).

[25] Hady, F., Ibrahim, F., El-Hawary, H., et al. “Forced convection flow of nanofluids past power-law stretching horizontal plates”, *Applied Mathematics*, **3**(2), pp. 121-126 (2012).

[26] Uddin, M. J., Rasel, S. K., Rahman, M. M., et al. “Natural convective heat transfer in a nanofluid-filled square vessel having a wavy upper surface in the presence of a magnetic field”, *Thermal Science and Engineering Progress*, **19**, pp. 100660 (2020).

[27] Cho, C.C. “Effects of a porous medium and wavy surface on heat transfer and entropy generation of Cu-water nanofluid natural convection in a square cavity containing partially-heated surface”, *International Communications in Heat and Mass Transfer*, **119**, pp. 104925 (2020).

[28] Misirlioglu, A., Baytas, A. C., and Pop, I. “Free convection in a wavy cavity filled with a porous medium”, *International Journal of Heat and Mass Transfer*, **48**(9), pp. 1840–1850 (2005).

[29] Sheremet, M. A., Oztop, H. F., and Pop, I. “MHD natural convection in an inclined wavy cavity with corner heater filled with a nanofluid”, *Journal of Magnetism and Magnetic Materials*, **416**, pp. 37–47 (2016).

[30] Ahmed, S. E., and Rashed, Z. Z. “MHD natural convection in a heat-generating porous medium-filled wavy enclosures using Buongiorno’s nanofluid model”, *Case Studies in Thermal Engineering*, **14**, pp. 100430 (2019).

[31] Abdulkadhim, A., Hamzah, H.K., Ali, F.H., *et al.* "Effect of heat generation and heat absorption on natural convection of Cu-water nanofluid in a wavy enclosure under magnetic field", *International Communications in Heat and Mass Transfer*, **120**, pp. 105024 (2021).

[32] Ahmed, S. E. "Effect of fractional derivatives on natural convection in a complex-wavy-wall surrounded enclosure filled with porous media using nanofluids", *ZAMM-Journal of Applied Mathematics and Mechanics/Zeitschrift für Angewandte Mathematik und Mechanik*, **100**(1), pp. e201800323 (2020).

[33] Hussain, S., Öztop, H. F., Mehmood, K., et al. "Effects of inclined magnetic field on mixed convection in a nanofluid filled the double lid-driven cavity with volumetric heat generation or absorption using finite element method", *Chinese Journal of Physics*, **56**(2), pp. 484–501 (2018).

[34] Yusuf, T. A., Mabood, F., Khan, W. A., et al. "Irreversibility analysis of Cu-TiO2-H2O hybrid-nanofluid impinging on a 3-D stretching sheet in a porous medium with non-linear radiation: Darcy-Forchhiemer's model", *Alexandria Engineering Journal*, **59**(6), pp. 5247–5261 (2020).

[35] Cheong, H. T., Sivasankaran, S., and Bhuvaneswari, M. "Natural convection in a wavy porous cavity with sinusoidal heating and internal heat generation", *International Journal of Numerical Methods for Heat & Fluid Flow*, **27**(2), pp. 287-309 (2017).

[36] Ahmed, S. E., Mansour, M. A., Rashad, A. M. , et al. "MHD natural convection from two heating modes in fined triangular enclosures filled with porous media using nanofluids", *Journal of Thermal Analysis and Calorimetry*, **139**(5), pp. 3133–3149 (2019).

Biographies:

Mohamed A. Mansour obtained his doctorate degree in applied Mathematics from Assuit University, Department of Mathematics, Faculty of Science, Egypt. He is a professor in the Department of Mathematics, Faculty of Science, Assuit University. His research interest is Mathematical methods, Fluid mechanics, and Mathematical modeling. He has several international publications in reputable Journals to his credit.

Sameh E. Ahmed obtained his doctorate degree in applied Mathematics from South Valley University, Department of Mathematics, Faculty of Science, Egypt. He is currently professor in the department of Mathematics, Faculty of science, King Khalid University. His research interest is in Mathematical methods, Fluid mechanics, Mathematical modelling. He has several international publications in reputable Journals to his credits.

Eman F. Mohamed obtained her Master's degree in Applied Mathematics from Assuit University, Department of Mathematics, Faculty of Science, Egypt. She is a teaching assistant in the Department of Basic Science, Faculty of Engineering, Sphinx University. Her research interest is Mathematical methods, Fluid mechanics, and Mathematical modeling.

Ahmed M. Ismaeel is currently a Lecturer of Applied Mathematics in the Faculty of Basic Sciences at King Salman International University, located in South Sinai, Egypt. His research primarily focuses on tackling intresting problems within the field of biology, particularly in the context of cancer treatment.

Previously, he held a Lecturer position at Assiut University from 2020 to 2021. In 2020, he successfully earned his PhD from the University of Glasgow, where he devoted his research to developing "A mathematical model for photothermal therapy of spherical tumors."

Table Captions:

Table 1. H_2O, Cu and TiO_2 thermo-physical properties [34].

Figure Captions:

Figure 1. The physical domain

Figure 2. (a) and (b) mapping of physical and computational models

Figure 3. Data validation. (A) the current results and (B) Cheong et al. [35].

Figure 4. (a) ContoursΨ, (b) T_f, (c) T_s, and (d) iso concentrations for Tio2–Cu/water Hybrid Nanofluid at$D = 0.5, Q = 1, \varepsilon = 0.5, \lambda = 2, Ha = 10, \phi_{cu} = \phi_{TiO2} = \frac{\phi}{2}, \phi = 0.05, H^* = 10, Da = 10^{-3}, \Phi = \pi/3$

Figure 5. (a) and (b) Profile of Nu_{sf} and Nu_{ss} with the heat source length for Tio2–Cu/water Hybrid Nanofluid at $D = 0.5, Q = 1, \varepsilon = 0.5, \lambda = 2, Ha = 10, \phi_{cu} = \phi_{TiO2} = \frac{\phi}{2}, \phi = 0.05, H^* = 10, Da = 10^{-3}, \Phi = \pi/3$

Figure 6. (a) Contours Ψ(b) T_f, (c) T_s and (d) iso concentrations for Tio2–Cu/water Hybrid Nanofluid at$B = 0.5, Q = 1, \varepsilon = 0.5, \lambda = 2, Ha = 10, \phi_{cu} = \phi_{TiO2} = \frac{\phi}{2}, \phi = 0.05, H^* = 10, Da = 10^{-3}, \Phi = \frac{\pi}{3}$

Figure 7. Profiles (a) and (b) of Nu_{sf} and Nu_{sf} with heat source position for Tio2–Cu/water Hybrid Nanofluid at $B = 0.5, Q = 1, \varepsilon = 0.5, \lambda = 2, Ha = 10, \phi_{cu} = \phi_{TiO2} = \frac{\phi}{2}, \phi = 0.05, H^* = 10, Da = 10^{-3}, \Phi = \frac{\pi}{3}$

Figure 8 (a) Contours Ψ, (b) T_f, (c) T_s, and (d) iso concentrations for Tio2–Cu/water Hybrid Nanofluid at $B = 0.5, D = 0.5, \varepsilon = 0.5, \lambda = 2, Ha = 10, \phi_{cu} = \phi_{TiO2} = \frac{\phi}{2}, \phi = 0.05, H^* = 10, Da = 10^{-3}, \Phi = \frac{\pi}{3}$

Figure 9. . Profiles of Nu_s along with heat generation parameter (Q) for Tio2–Cu/water Hybrid Nanofluid at $B = 0.5, D = 0.5, \varepsilon = 0.5, \lambda = 2, Ha = 10, \phi_{cu} = \phi_{TiO2} = \frac{\phi}{2}, \phi = 0.05, H^* = 10, Da = 10^{-3}, \Phi = \frac{\pi}{3}$

Figure 10. (a) Contours Ψ, (b) T_f, (c) T_s, and (d) iso concentrations for Tio2–Cu/water Hybrid Nano fluid at $B = 0.5, Q = 1, \varepsilon = 0.5, \lambda = 2, D = 0.5, \phi_{cu} = \phi_{TiO2} = \frac{\phi}{2}, \phi = 0.05, H^* = 10, Da = 10^{-3}, \Phi = \frac{\pi}{3}$

Figure 11. Profiles (a) and (b) of Nu_{sf} and Nu_{sf} with Hartman number Ha for Tio2–Cu/water Hybrid Nanofluid at $B = 0.5, Q = 1, \varepsilon = 0.5, \lambda = 2, D = 0.5, \phi_{cu} = \phi_{TiO2} = \frac{\phi}{2}, \phi = 0.05, H^* = 10, Da = 10^{-3}, \Phi = \frac{\pi}{3}$

Figure 12. (a) Contours Ψ, (b) T_f, (c) T_s, and (d) iso concentrations for Tio2–Cu/water Hybrid Nanofluid at $B = 0.5, Q = 1, \varepsilon = 0.5, D = 0.5, \phi_{cu} = \phi_{TiO2} = \frac{\phi}{2}, \phi = 0.05, Ha = 10, H^* = 10, Da = 10^{-3}, \Phi = \frac{\pi}{3}$

Figure 13. . Profiles (a) and (b) of Nu_{sf} and Nu_{sf} with undulation Parameter (λ) for Tio2–Cu/water Hybrid Nanofluid at $B = 0.5, Q = 1, \varepsilon = 0.5, D = 0.5, \phi_{cu} = \phi_{TiO2} = \frac{\phi}{2}, \phi = 0.05, H^* = 10, Ha = 10, Da = 10^{-3}, \Phi = \frac{\pi}{3}$

Figure 14. Profiles of Nu_{fs} with H^* for Tio2–Cu/water Hybrid Nanofluid at

$B = 0.5, D = 0.5\ Q = 1, \varepsilon = 0.5, \lambda = 2, D = 0.5, Ha = 10, \phi_{cu} = \phi_{TiO2} = \frac{\phi}{2}, \phi = 0.05$

Figure 15. Variation of Nu_m with H^* at $B = 0.5, Q = 1, \varepsilon = 0.5, \lambda = 2, D = 0.5, \phi_{cu} = \phi_{TiO2} = \frac{\phi}{2}, \phi = 0.05, Da = 10^{-3}, \Phi = \frac{\pi}{3}$

Figure 16. Profiles of (a) Nu_{sf} and (b) Nu_{sf} with the volume of nanoparticles for Tio2–Cu/water Hybrid Nanofluid at $B = 0.5, Q = 1, \varepsilon = 0.5, \lambda = 2, D = 0.5, , H^* = 10, Ha = 10, Da = 10^{-3}, \Phi = \frac{\pi}{3}$

Figure 17. (a) Contours Ψ, (b) T_f, (c) T_s, and (d) iso concentrations for Tio2–Cu/water Hybrid Nanofluid at $B = 0.5, Q = 1, \varepsilon = 0.5, \lambda = 2, D = 0.5, \phi_{cu} = \phi_{TiO2} = \frac{\phi}{2}, \phi = 0.05, H^* = 10, Ha = 10, \Phi = \frac{\pi}{3}$

Figure 18. Variation Nu_m of fluid phase (a) and solid phase (b) with Darcy parameter for Tio2–Cu/water Hybrid Nanofluid at$B = 0.5, Q = 1, \varepsilon = 0.5, \lambda = 2, D = 0.5, \phi_{cu} = \phi_{TiO2} = \frac{\phi}{2}, \phi = 0.05, H^* = 10, Ha = 10, \Phi = \pi/3$

Figure 19. Profiles (a) and (b) of Nu_{sf} and Nu_{sf} with inclination angle Φ for Tio2–Cu/water Hybrid Nanofluid at $B = 0.5, Q = 1, \varepsilon = 0.5, \lambda = 2, D = 0.5, \phi_{cu} = \phi_{TiO2} = \frac{\phi}{2}, \phi = 0.05, H^* = 10, Ha = 10$

Physical properties	Water	Copper (Cu)	Titanium dioxide (TiO_2)
$\rho\left(\frac{kg}{m^3}\right)$	997.1	8933	4250
$C_p\left(\frac{J}{kg\,K}\right)$	4179	385	686.2
$k\left(\frac{W}{m\,K}\right)$	0.613	401	8.9538
$\beta_T \times 10^{-5}\left(\frac{1}{K}\right)$	21	1.67	0.9
$\sigma(S/m)$	0.05	5.96×10^{-7}	1×10^{-12}

Table 1.

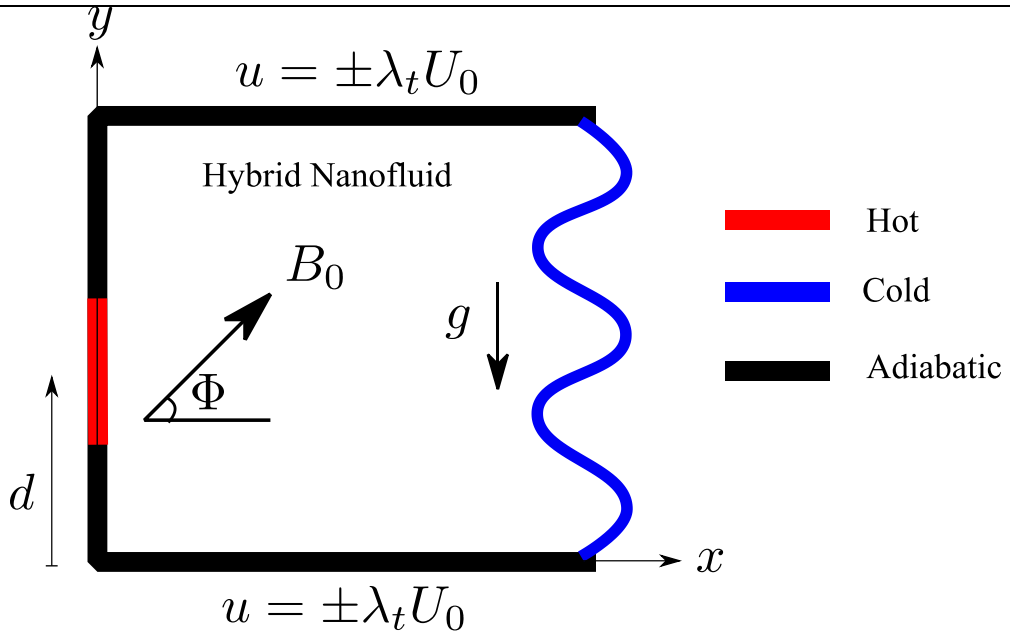

Figure 1

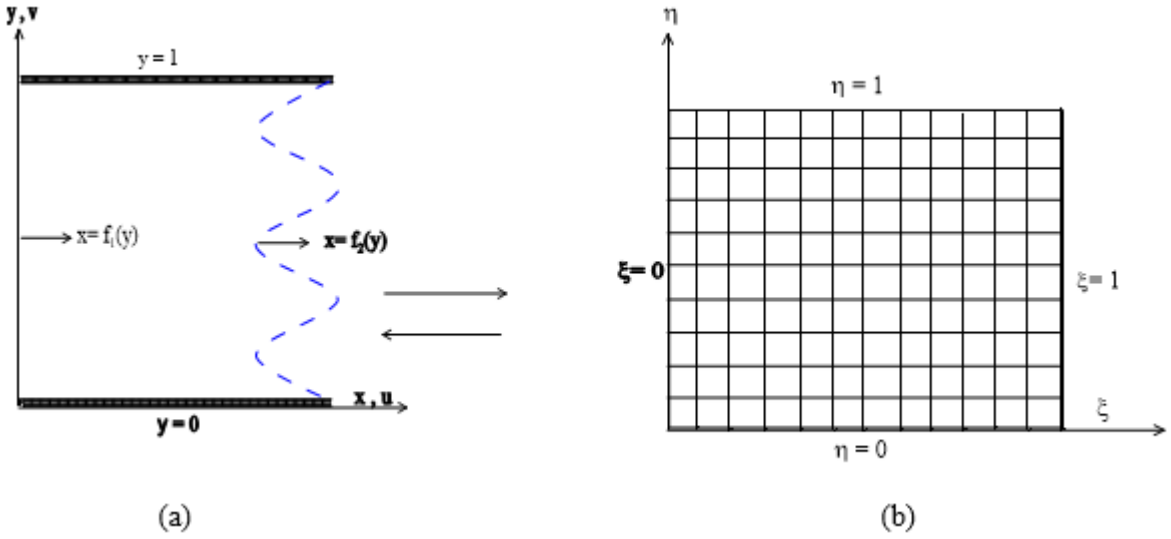

Figure 2

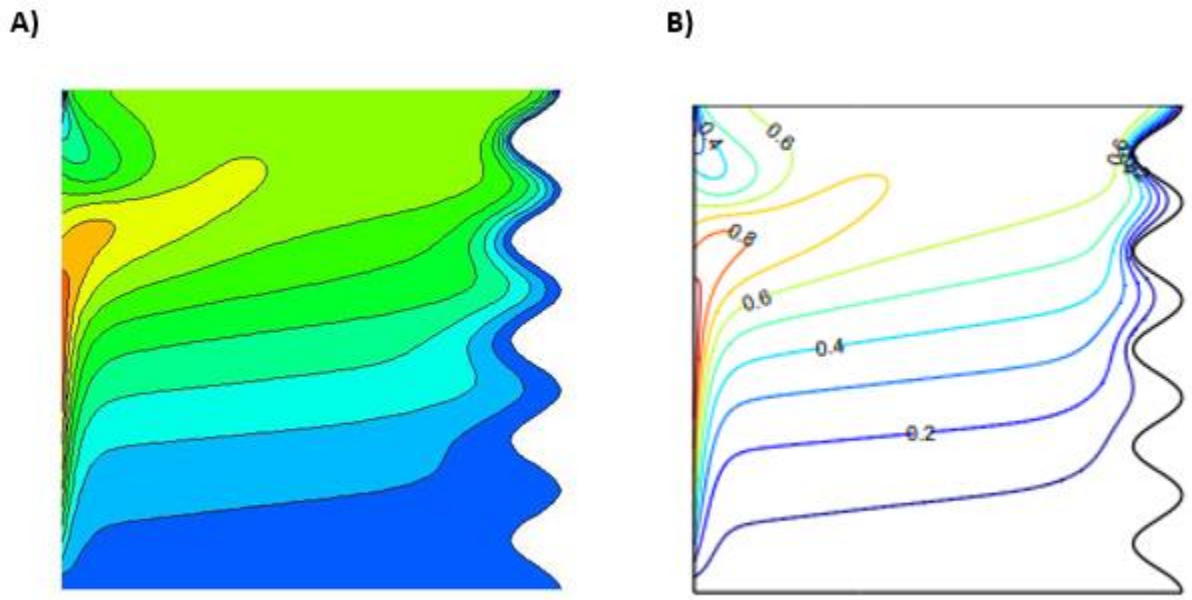
A)
B)
0.8
0.6
0.4
0.2

Figure 3

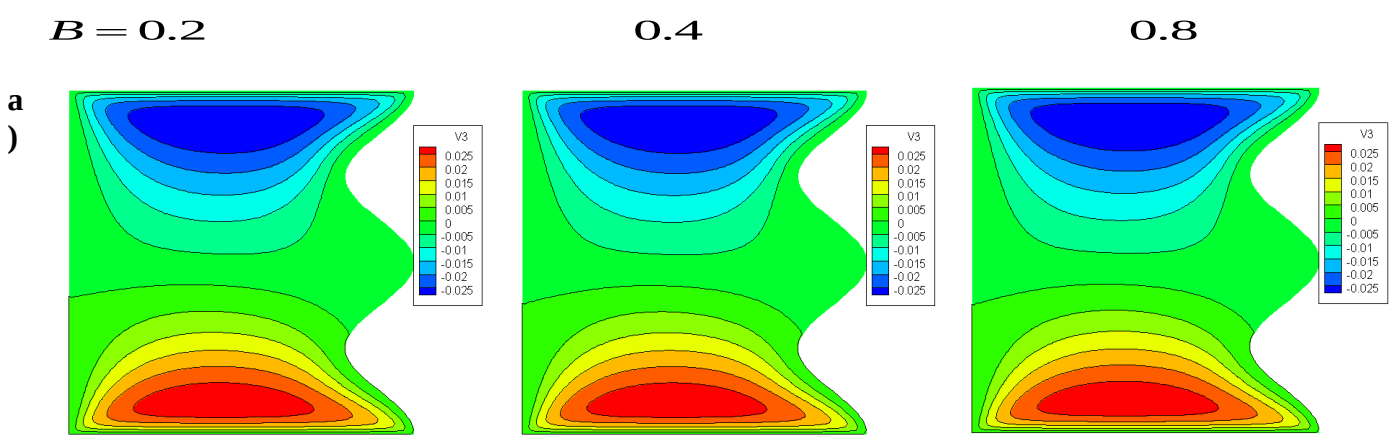
$B = 0.2$
0.4
0.8
a)
V3
0.025
0.02
0.015
0.01
0.005
0
-0.005
-0.01
-0.015
-0.02
-0.025

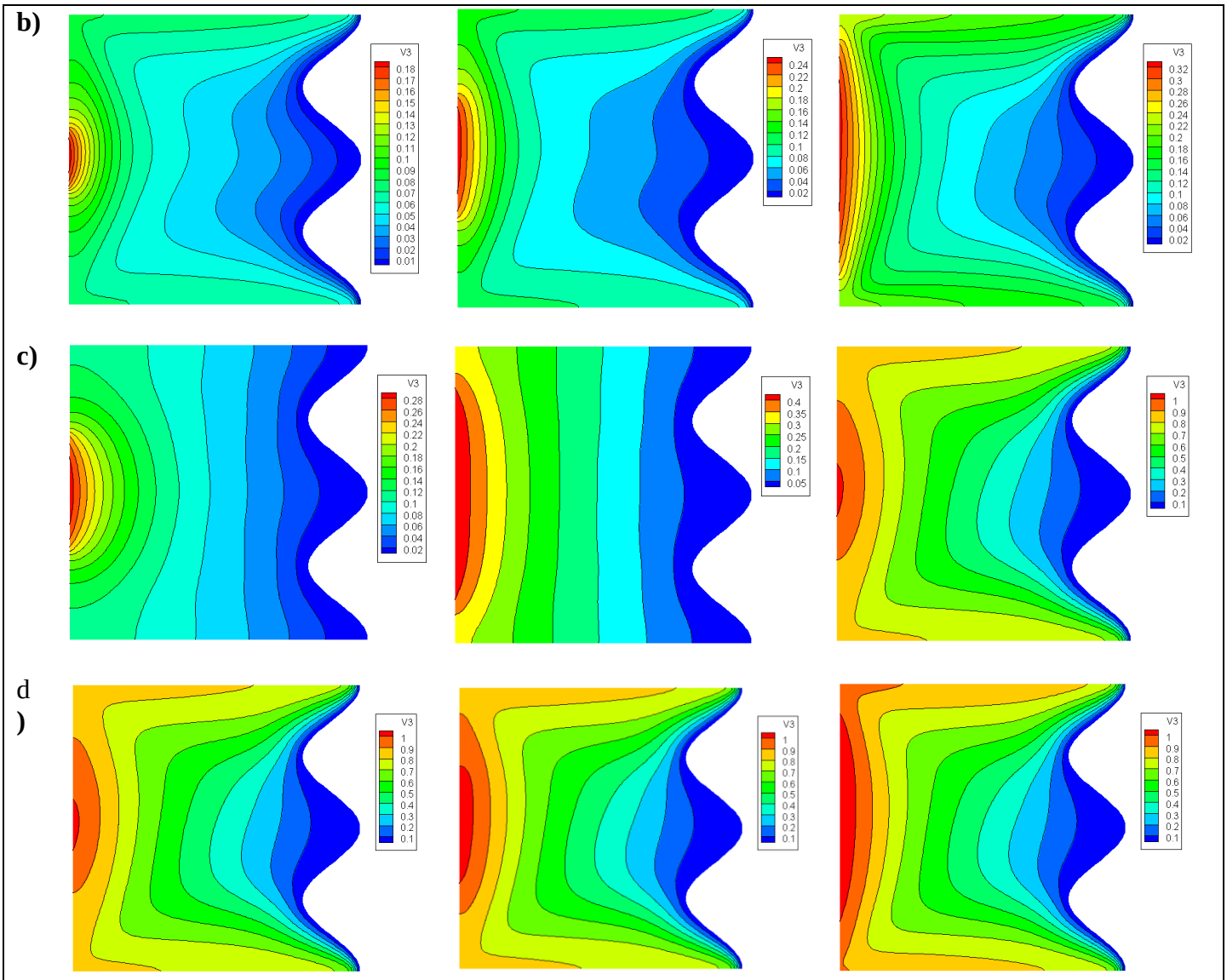
b)
V3
0.18
0.17
0.16
0.15
0.14
0.13
0.12
0.11
0.1
0.09
0.08
0.07
0.06
0.05
0.04
0.03
0.02
0.01
V3
0.24
0.22
0.2
0.18
0.16
0.14
0.12
0.1
0.08
0.06
0.04
0.02
V3
0.32
0.3
0.28
0.26
0.24
0.22
0.2
0.18
0.16
0.14
0.12
0.1
0.08
0.06
0.04
0.02
c)
V3
0.28
0.26
0.24
0.22
0.2
0.18
0.16
0.14
0.12
0.1
0.08
0.06
0.04
0.02
V3
0.4
0.35
0.3
0.25
0.2
0.15
0.1
0.05
V3
1
0.9
0.8
0.7
0.6
0.5
0.4
0.3
0.2
0.1
d
)
V3
1
0.9
0.8
0.7
0.6
0.5
0.4
0.3
0.2
0.1
V3
1
0.9
0.8
0.7
0.6
0.5
0.4
0.3
0.2
0.1
V3
1
0.9
0.8
0.7
0.6
0.5
0.4
0.3
0.2
0.1

Figure 4

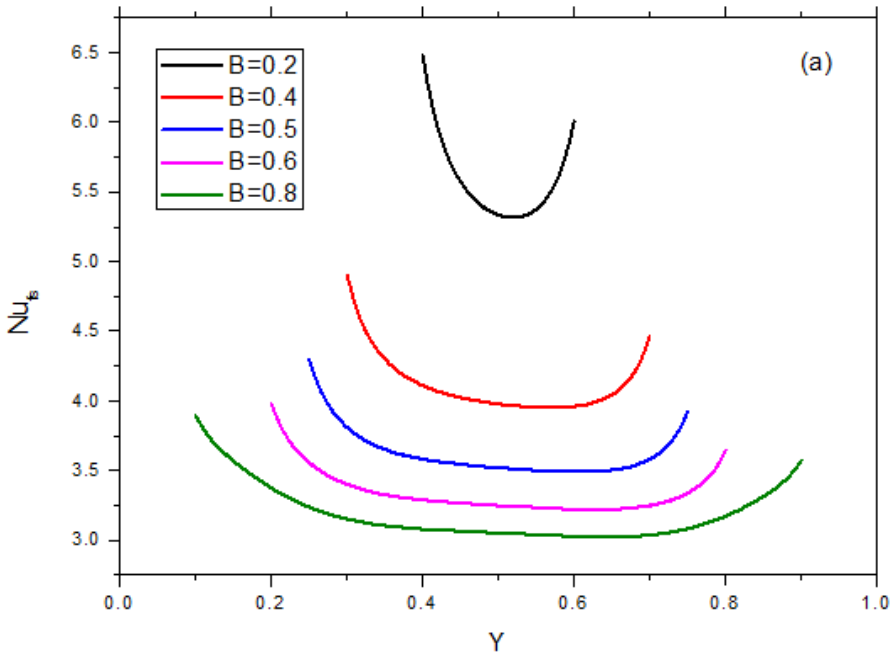
B=0.2
B=0.4
B=0.5
B=0.6
B=0.8
(a)
Nu_fs
Y
6.5
6.0
5.5
5.0
4.5
4.0
3.5
3.0
0.0
0.2
0.4
0.6
0.8
1.0

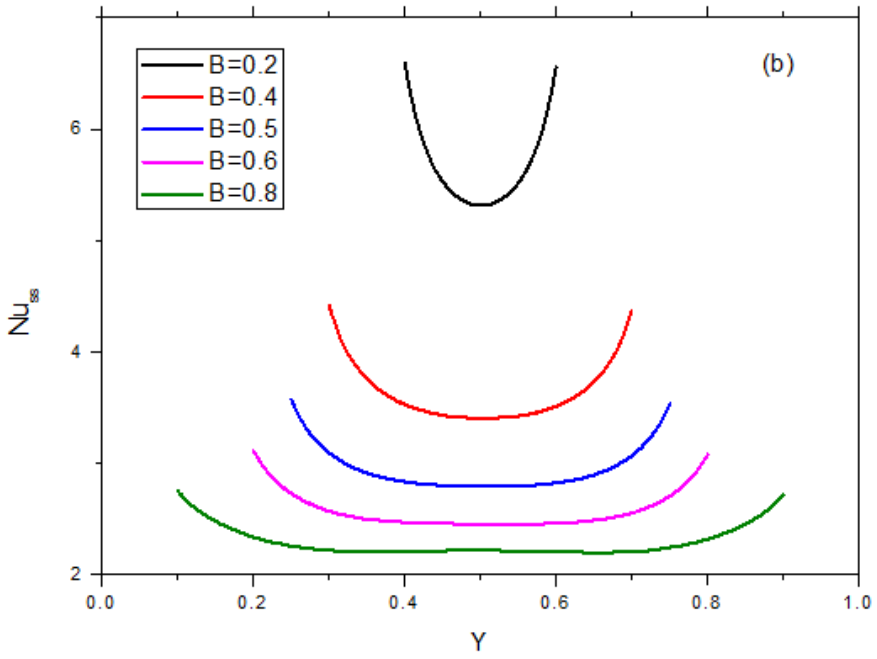
B=0.2
B=0.4
B=0.5
B=0.6
B=0.8
(b)
Nu_ss
Y
6
4
2
0.0
0.2
0.4
0.6
0.8
1.0

Figure 5

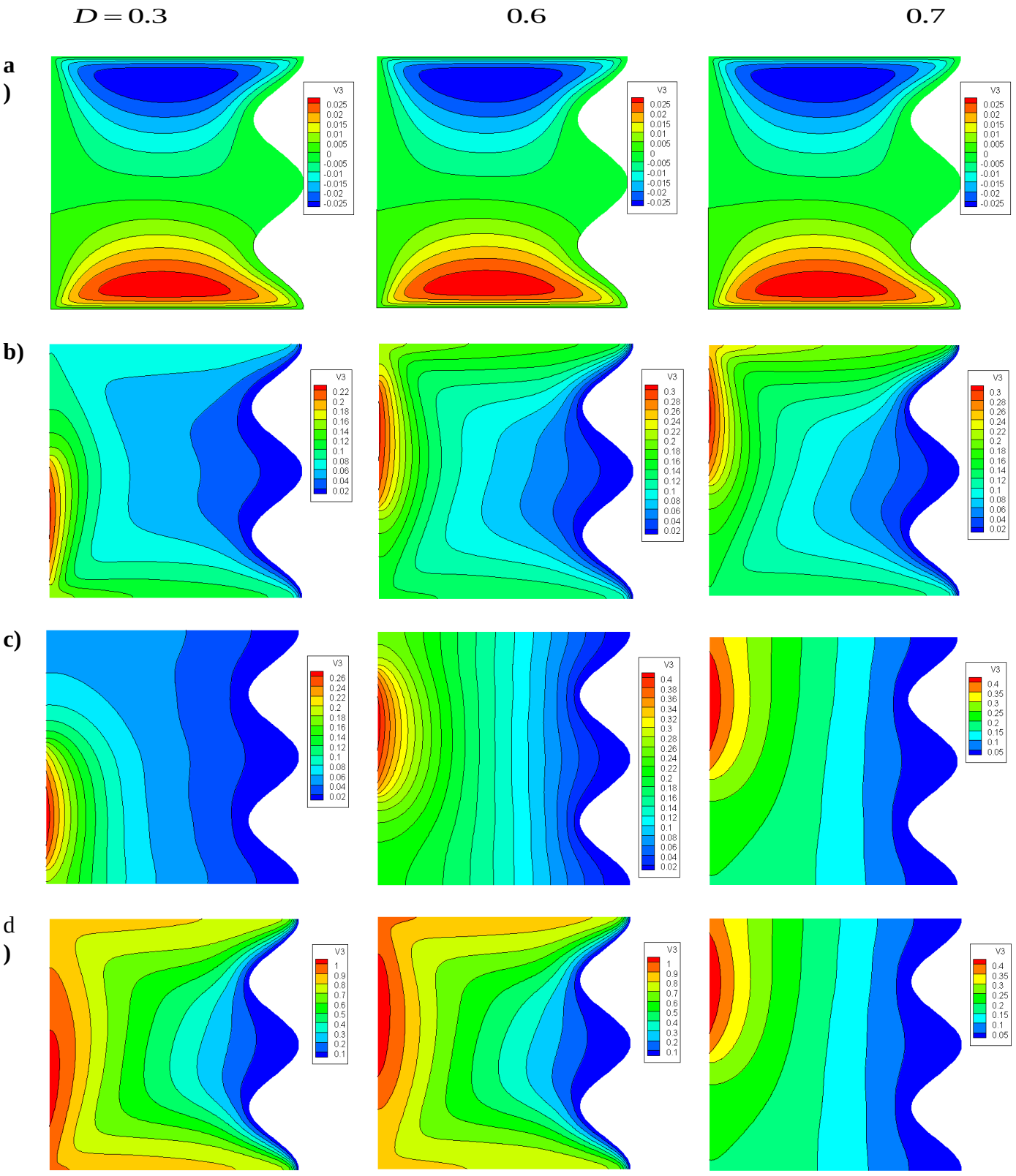

Figure 6

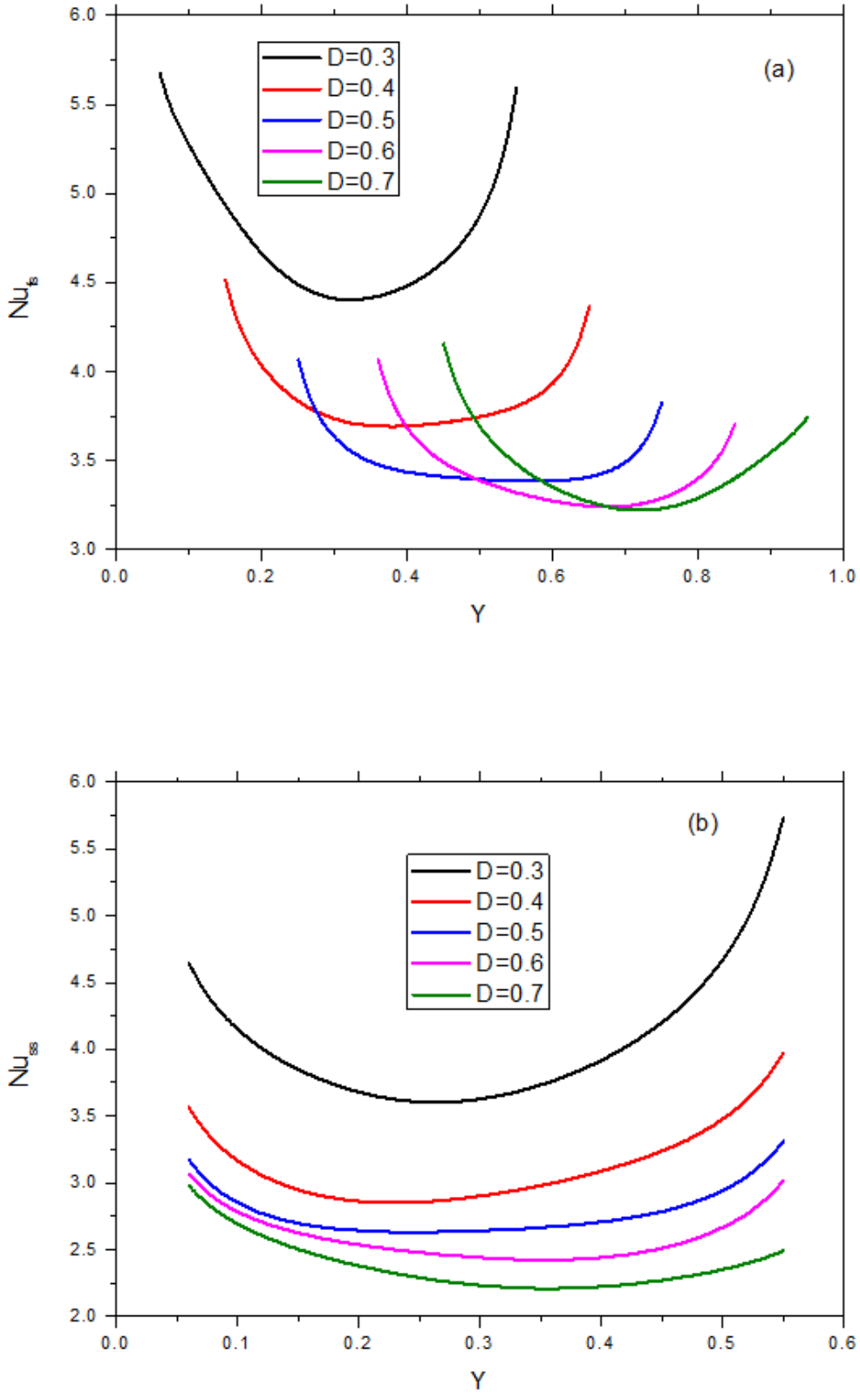
(a)
D=0.3
D=0.4
D=0.5
D=0.6
D=0.7
Nu_fs
Y
6.0
5.5
5.0
4.5
4.0
3.5
3.0
0.0
0.2
0.4
0.6
0.8
1.0
(b)
D=0.3
D=0.4
D=0.5
D=0.6
D=0.7
Nu_ss
Y
6.0
5.5
5.0
4.5
4.0
3.5
3.0
2.5
2.0
0.0
0.1
0.2
0.3
0.4
0.5
0.6

Figure 7

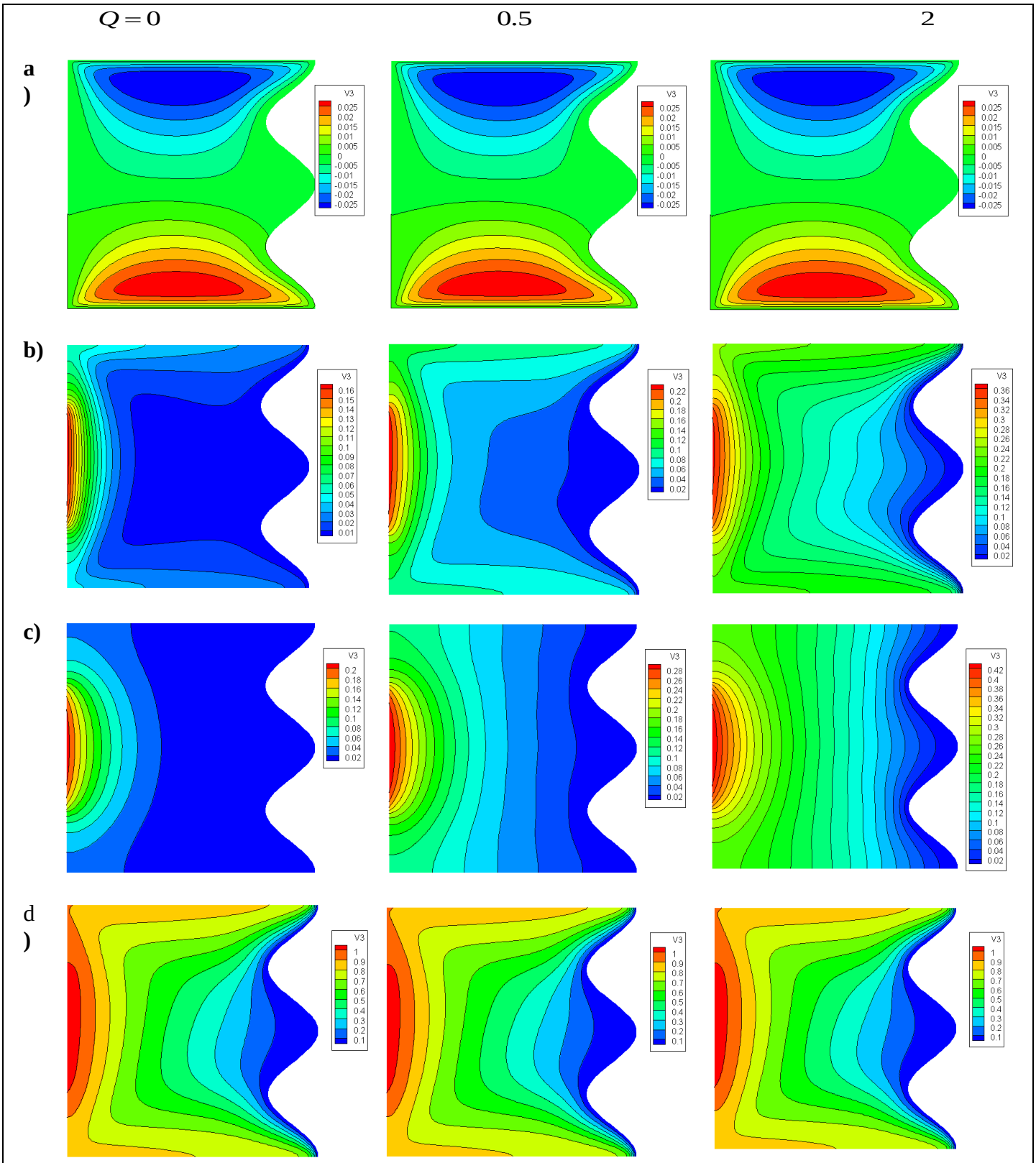

Figure 8

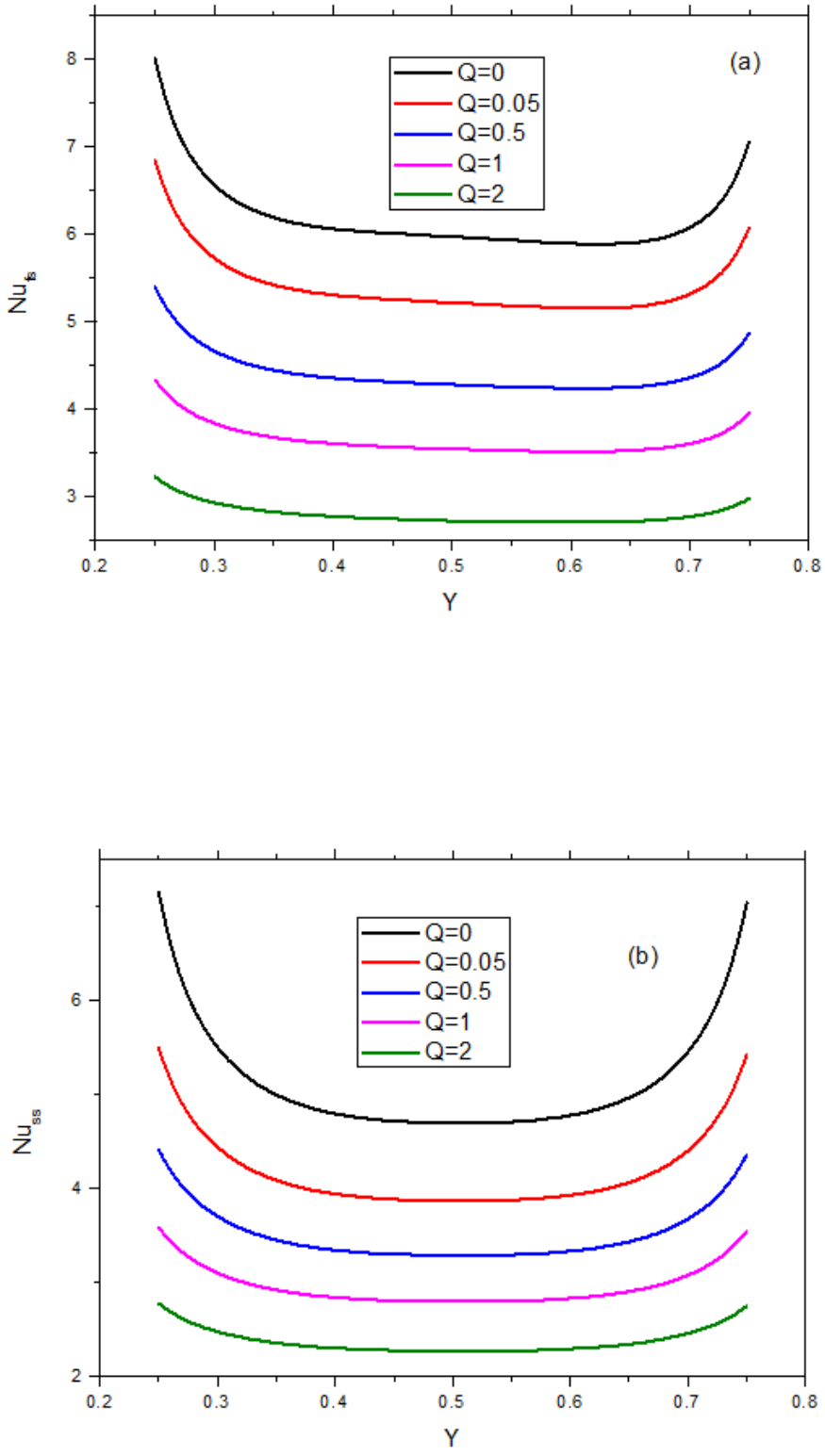

Figure 9

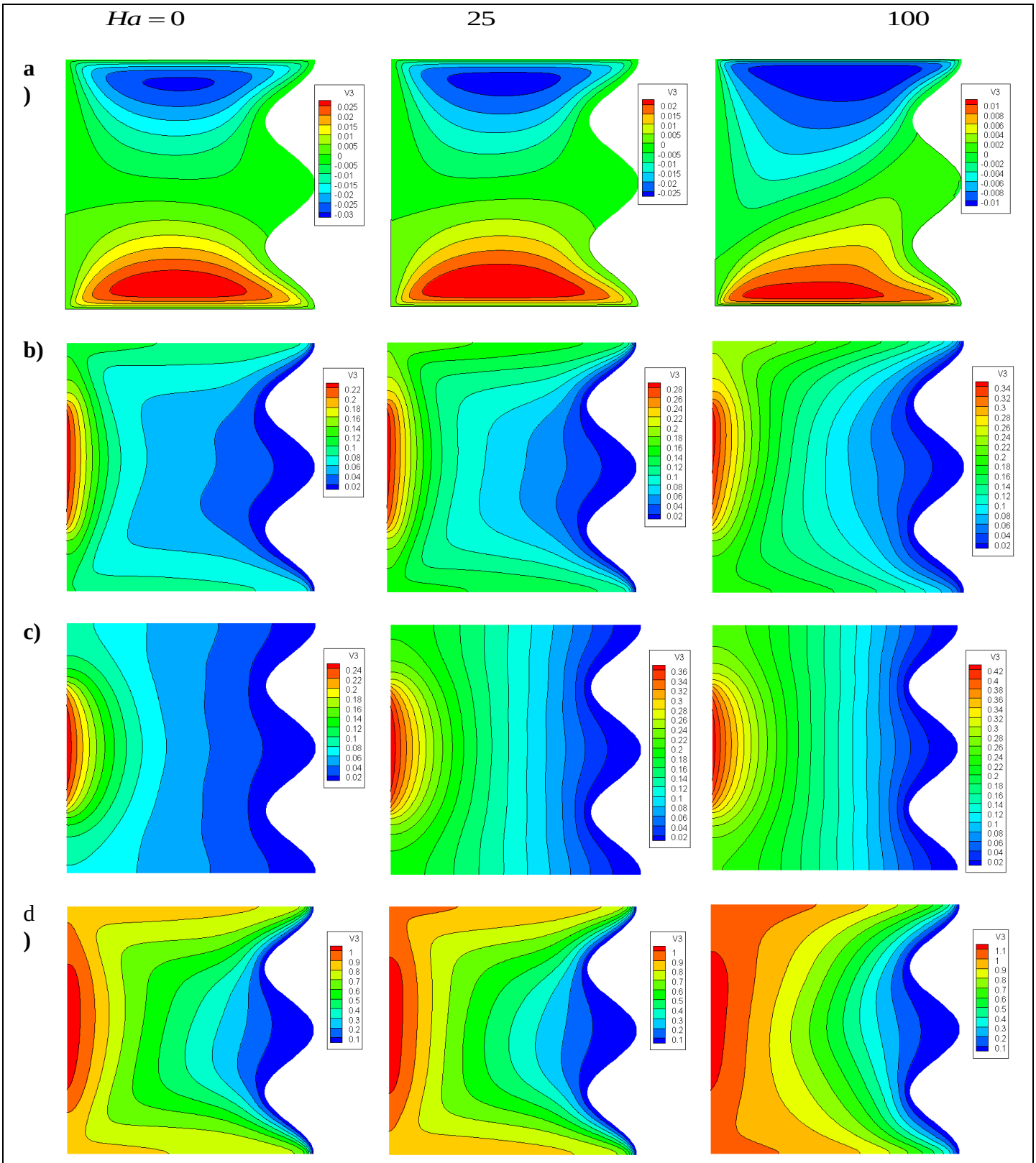

Figure 10

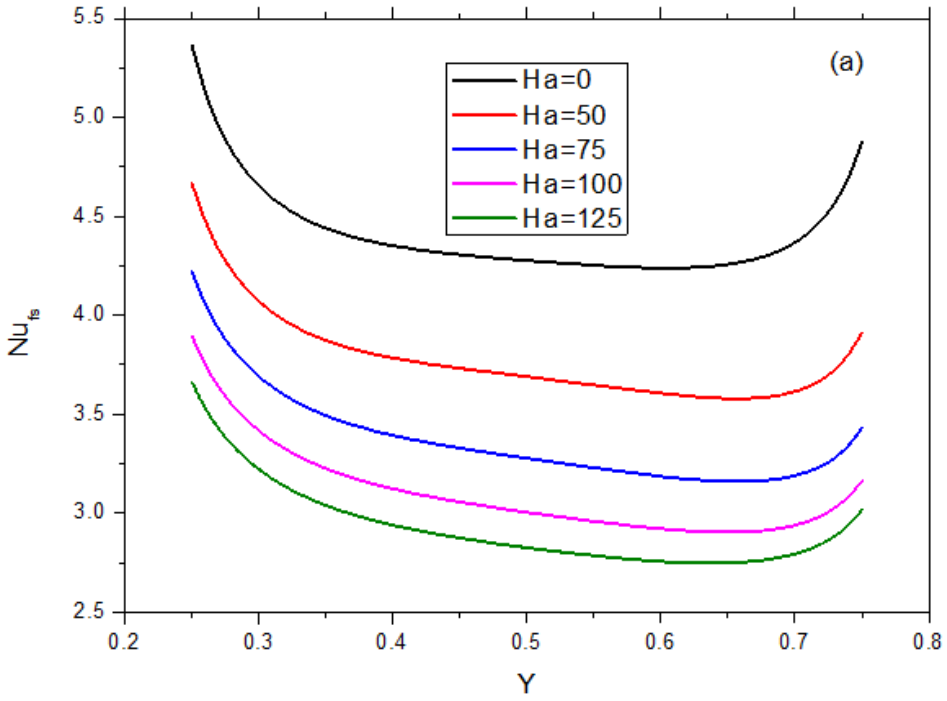
(a)
Ha=0
Ha=50
Ha=75
Ha=100
Ha=125
Nu_fs
Y
5.5
5.0
4.5
4.0
3.5
3.0
2.5
0.2
0.3
0.4
0.5
0.6
0.7
0.8

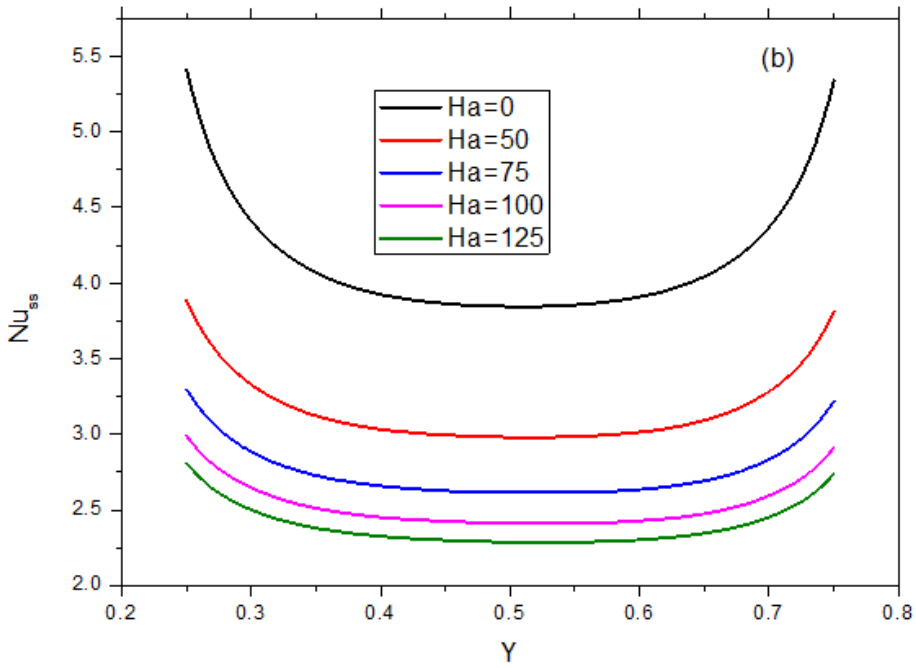
(b)
Ha=0
Ha=50
Ha=75
Ha=100
Ha=125
Nu_ss
Y
5.5
5.0
4.5
4.0
3.5
3.0
2.5
2.0
0.2
0.3
0.4
0.5
0.6
0.7
0.8

Figure 11

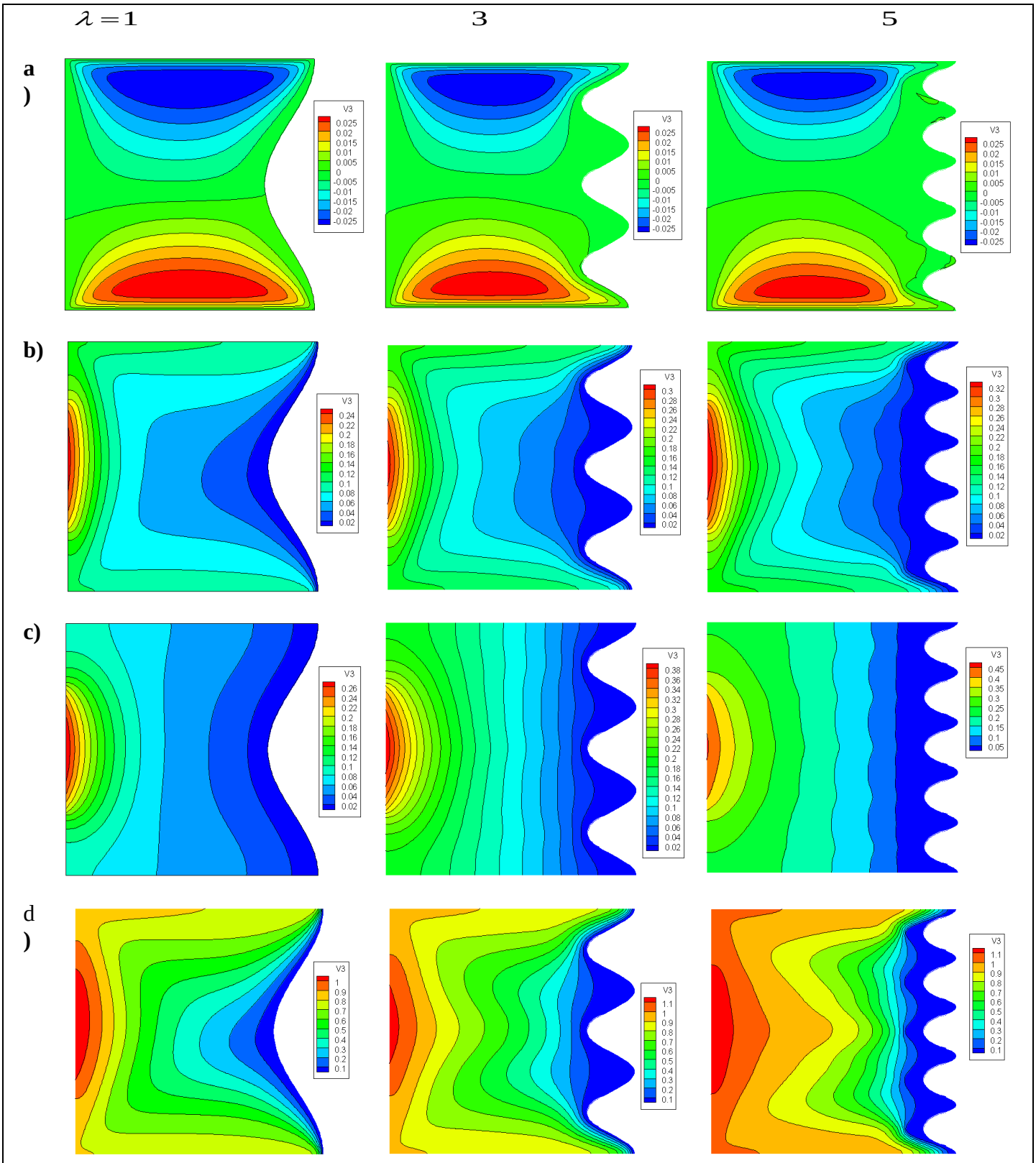
λ = 1
3
5
a)
b)
c)
d)
V3
0.025
0.02
0.015
0.01
0.005
0
-0.005
-0.01
-0.015
-0.02
-0.025
0.24
0.22
0.2
0.18
0.16
0.14
0.12
0.1
0.08
0.06
0.04
0.02
0.3
0.28
0.26
0.24
0.22
0.2
0.18
0.16
0.14
0.12
0.1
0.08
0.06
0.04
0.02
0.32
0.3
0.28
0.26
0.24
0.22
0.2
0.18
0.16
0.14
0.12
0.1
0.08
0.06
0.04
0.02
0.26
0.24
0.22
0.2
0.18
0.16
0.14
0.12
0.1
0.08
0.06
0.04
0.02
0.38
0.36
0.34
0.32
0.3
0.28
0.26
0.24
0.22
0.2
0.18
0.16
0.14
0.12
0.1
0.08
0.06
0.04
0.02
0.45
0.4
0.35
0.3
0.25
0.2
0.15
0.1
0.05
1
0.9
0.8
0.7
0.6
0.5
0.4
0.3
0.2
0.1
1.1
1
0.9
0.8
0.7
0.6
0.5
0.4
0.3
0.2
0.1
1.1
1
0.9
0.8
0.7
0.6
0.5
0.4
0.3
0.2
0.1

Figure 12

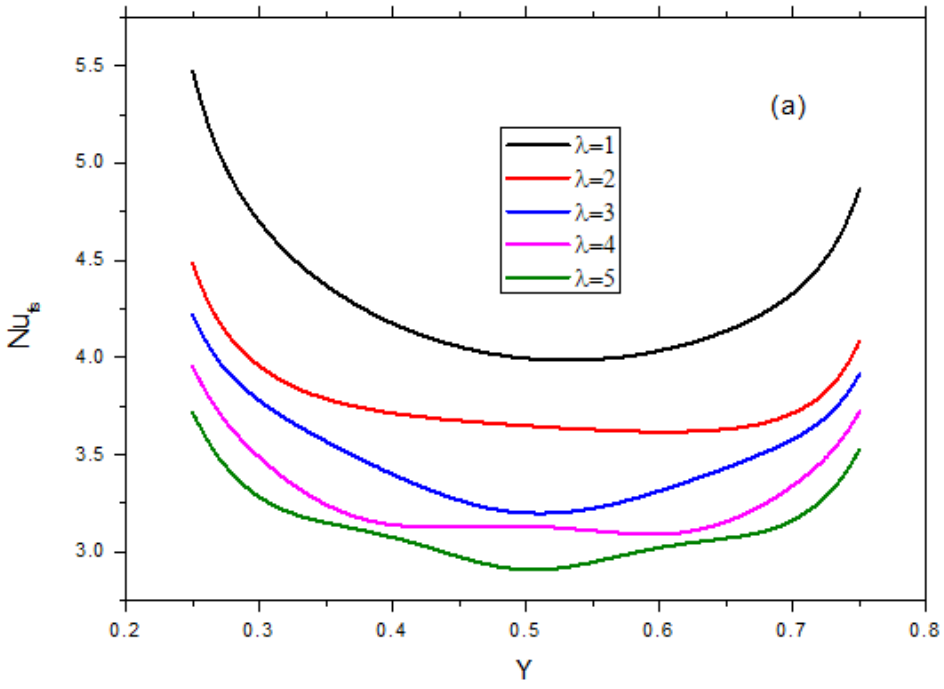
(a)
λ=1
λ=2
λ=3
λ=4
λ=5
Nu_fs
Y
5.5
5.0
4.5
4.0
3.5
3.0
0.2
0.3
0.4
0.5
0.6
0.7
0.8

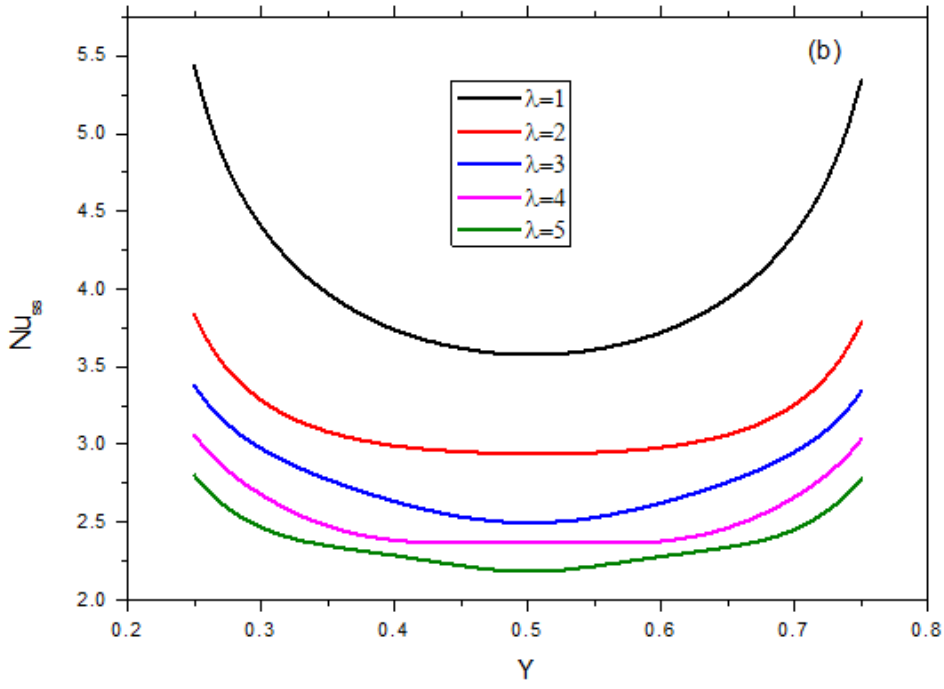
(b)
λ=1
λ=2
λ=3
λ=4
λ=5
Nu_ss
Y
5.5
5.0
4.5
4.0
3.5
3.0
2.5
2.0
0.2
0.3
0.4
0.5
0.6
0.7
0.8

Figure 13

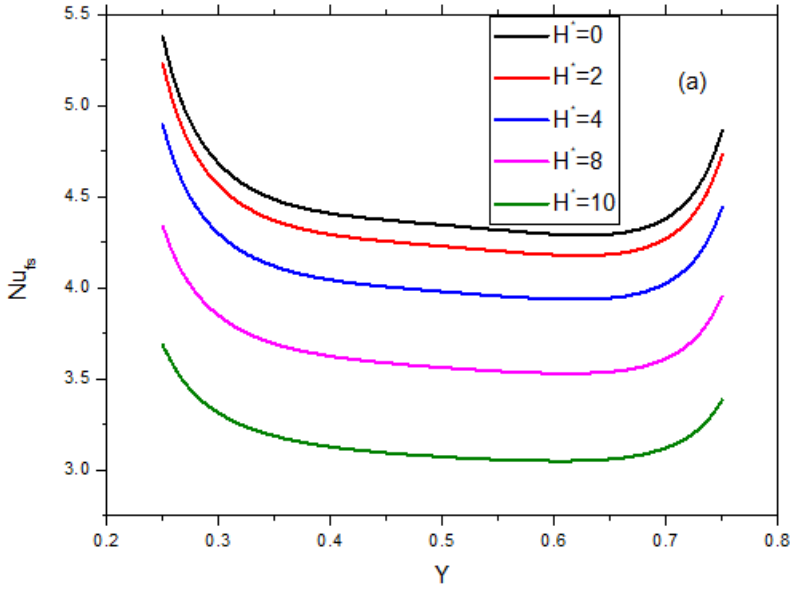

Figure 14

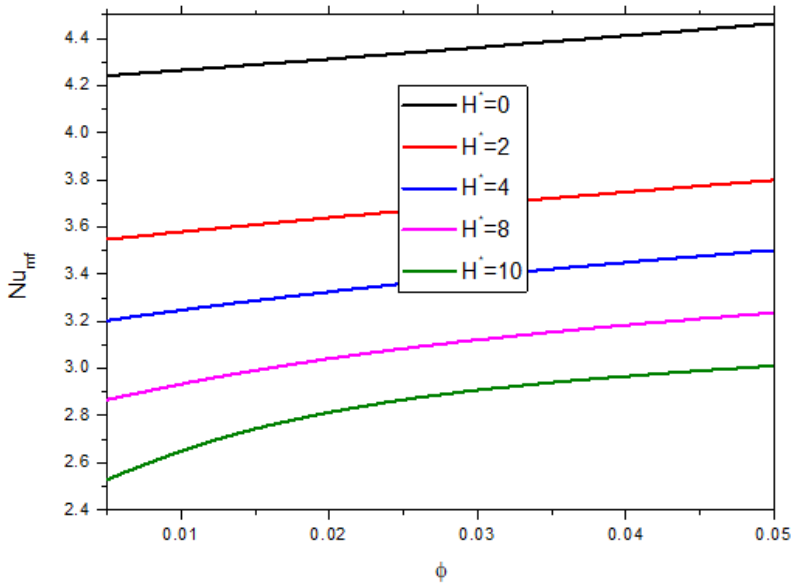

Figure 15

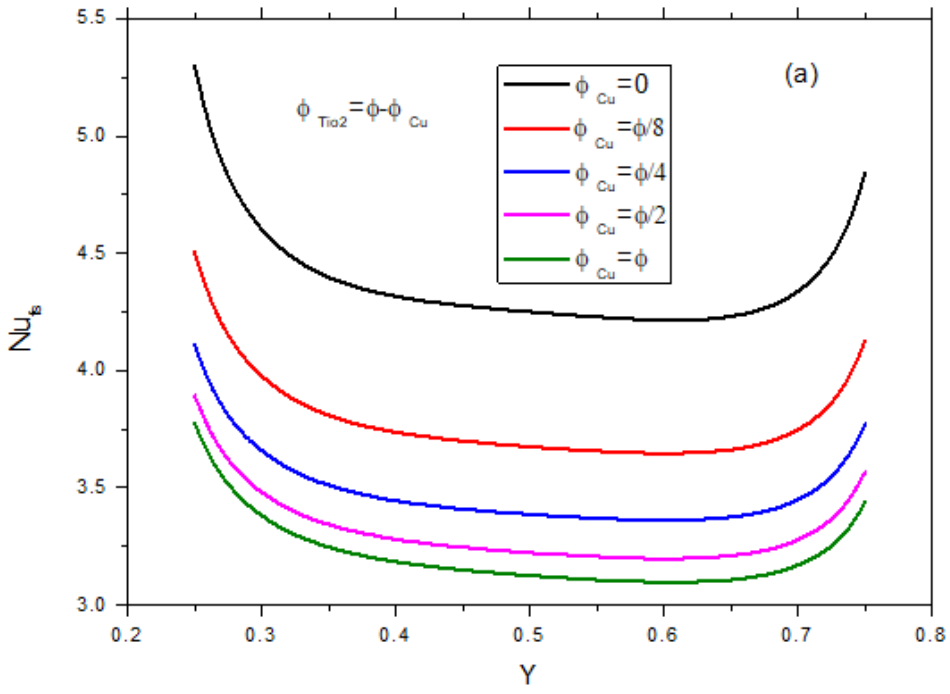
(a)
$\phi_{Tio2}=\phi-\phi_{Cu}$
$\phi_{Cu}=0$
$\phi_{Cu}=\phi/8$
$\phi_{Cu}=\phi/4$
$\phi_{Cu}=\phi/2$
$\phi_{Cu}=\phi$
Nu_{ss}
Y
5.5
5.0
4.5
4.0
3.5
3.0
0.2
0.3
0.4
0.5
0.6
0.7
0.8

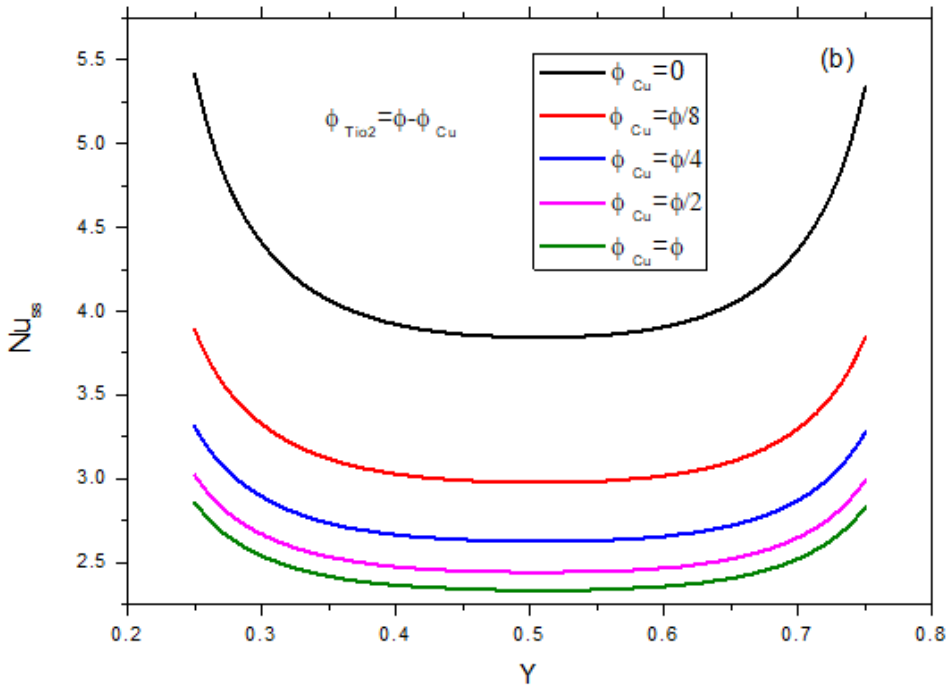
(b)
$\phi_{Tio2}=\phi-\phi_{Cu}$
$\phi_{Cu}=0$
$\phi_{Cu}=\phi/8$
$\phi_{Cu}=\phi/4$
$\phi_{Cu}=\phi/2$
$\phi_{Cu}=\phi$
Nu_{ss}
Y
5.5
5.0
4.5
4.0
3.5
3.0
2.5
0.2
0.3
0.4
0.5
0.6
0.7
0.8

Figure 16

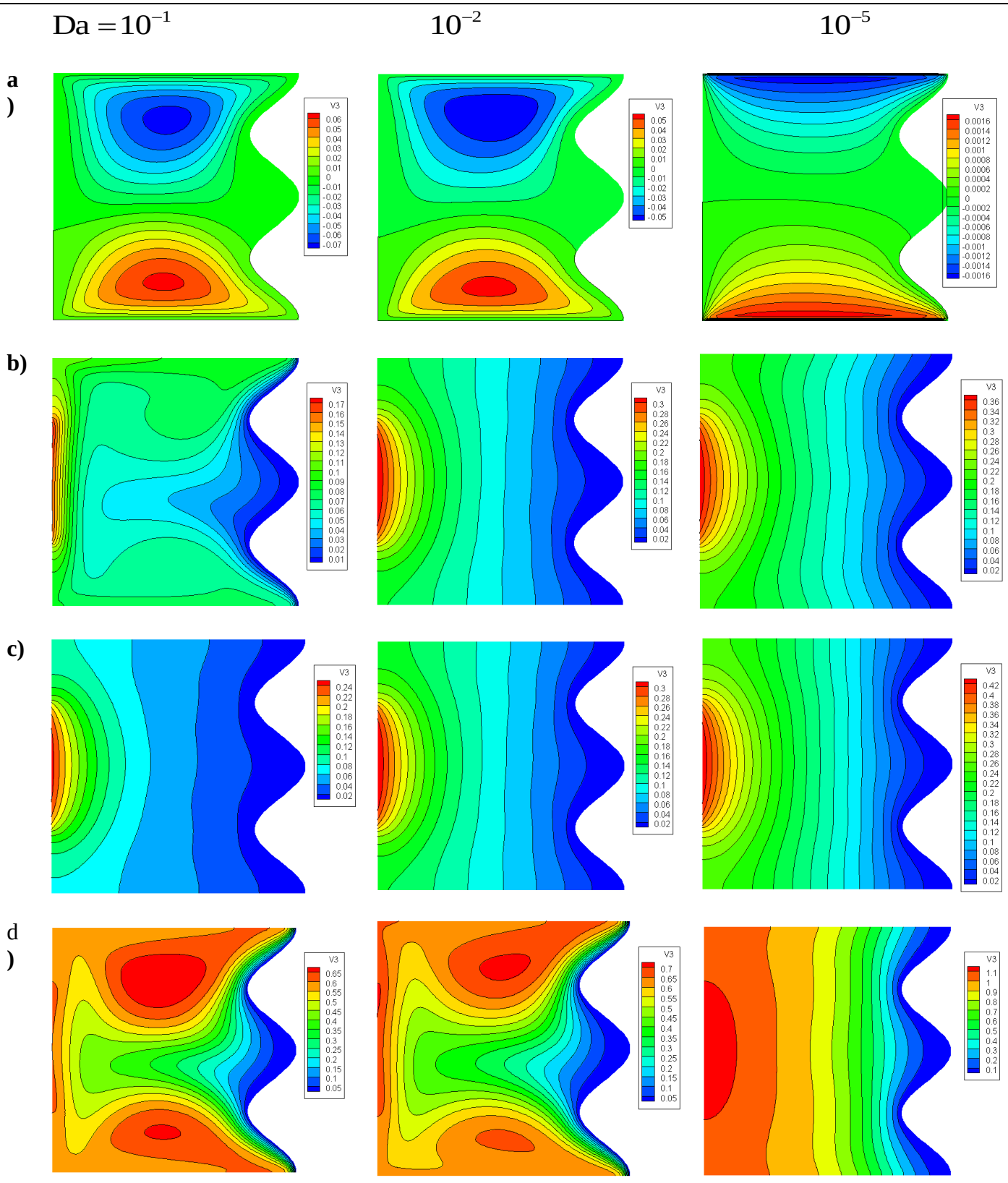

Figure 17

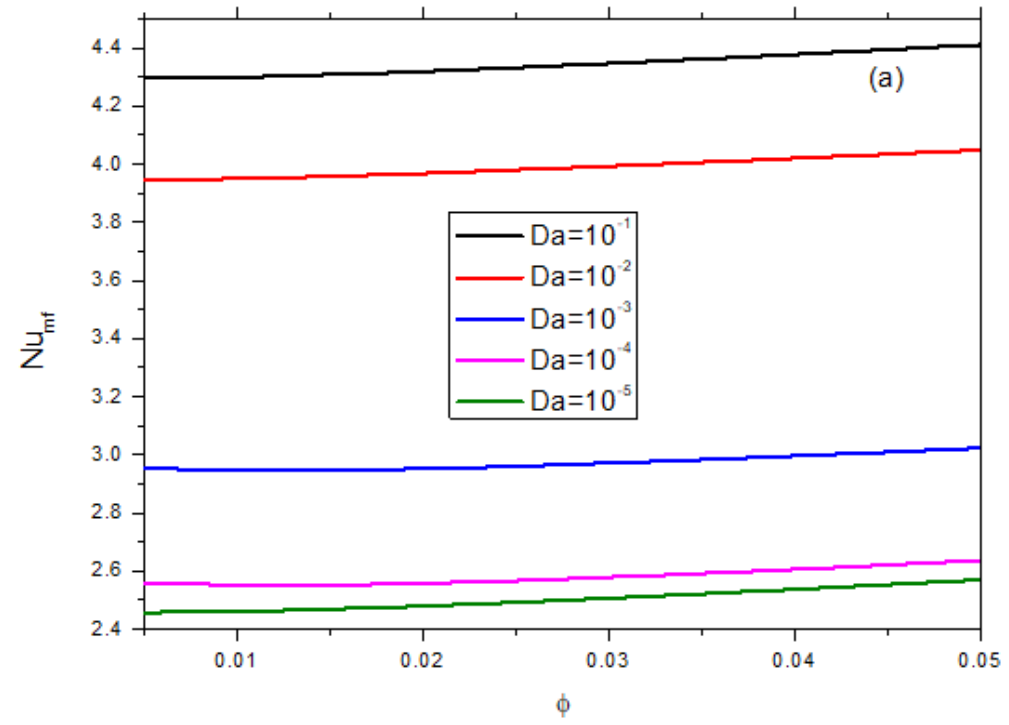
(a)
Da=10^-1
Da=10^-2
Da=10^-3
Da=10^-4
Da=10^-5
Nu_mf
ϕ
4.4
4.2
4.0
3.8
3.6
3.4
3.2
3.0
2.8
2.6
2.4
0.01
0.02
0.03
0.04
0.05

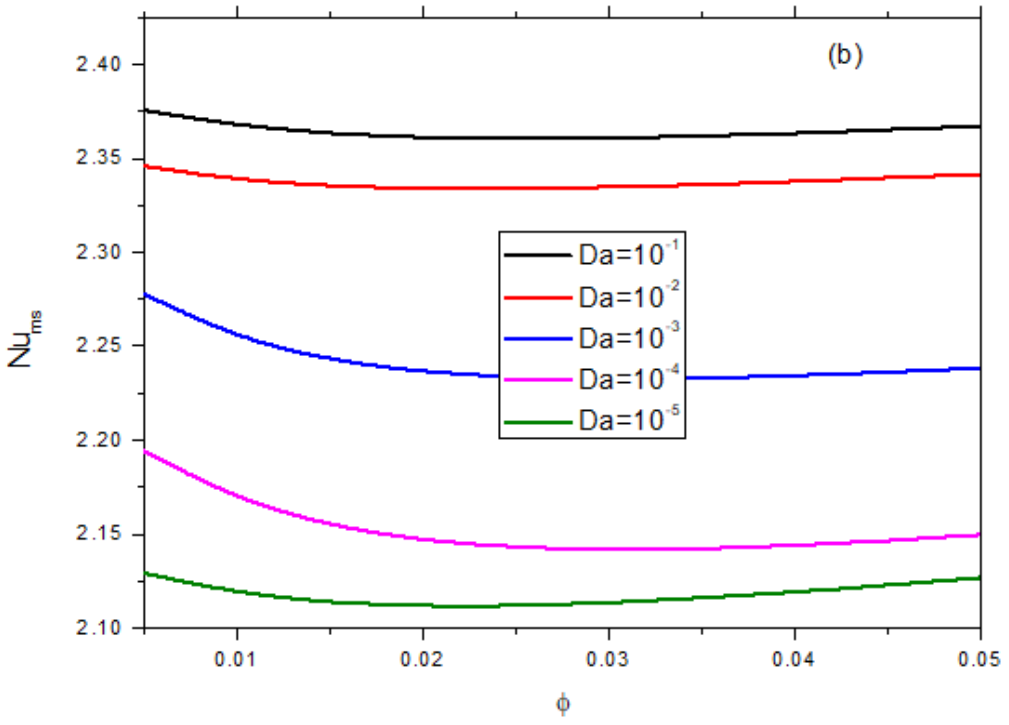
(b)
Da=10^-1
Da=10^-2
Da=10^-3
Da=10^-4
Da=10^-5
Nu_ms
ϕ
2.40
2.35
2.30
2.25
2.20
2.15
2.10
0.01
0.02
0.03
0.04
0.05

Figure18

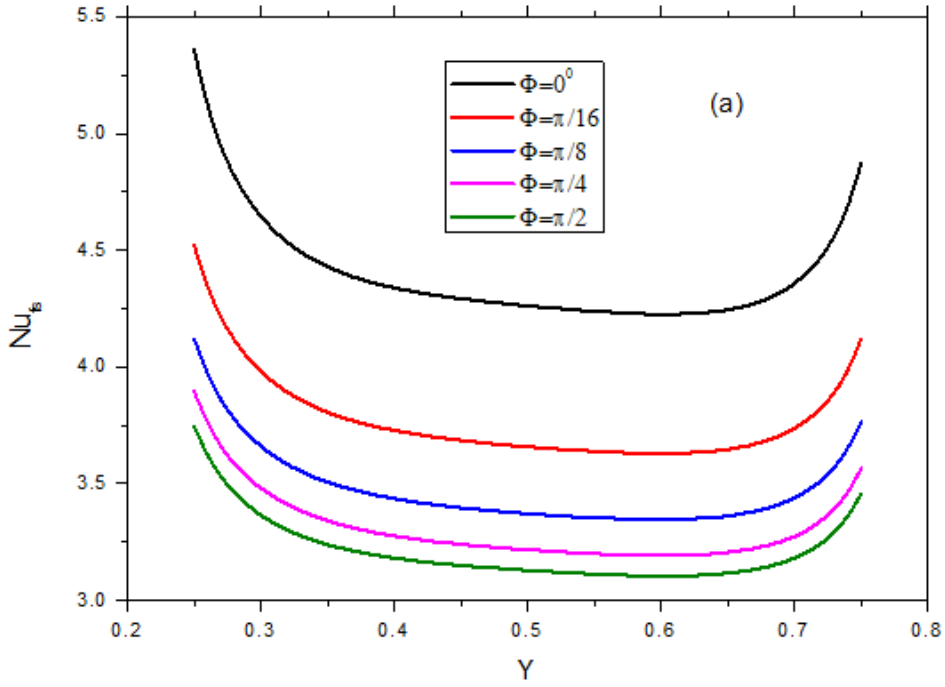
(a)
Φ=0⁰
Φ=π/16
Φ=π/8
Φ=π/4
Φ=π/2
Nu_s
Y
5.5
5.0
4.5
4.0
3.5
3.0
0.2
0.3
0.4
0.5
0.6
0.7
0.8

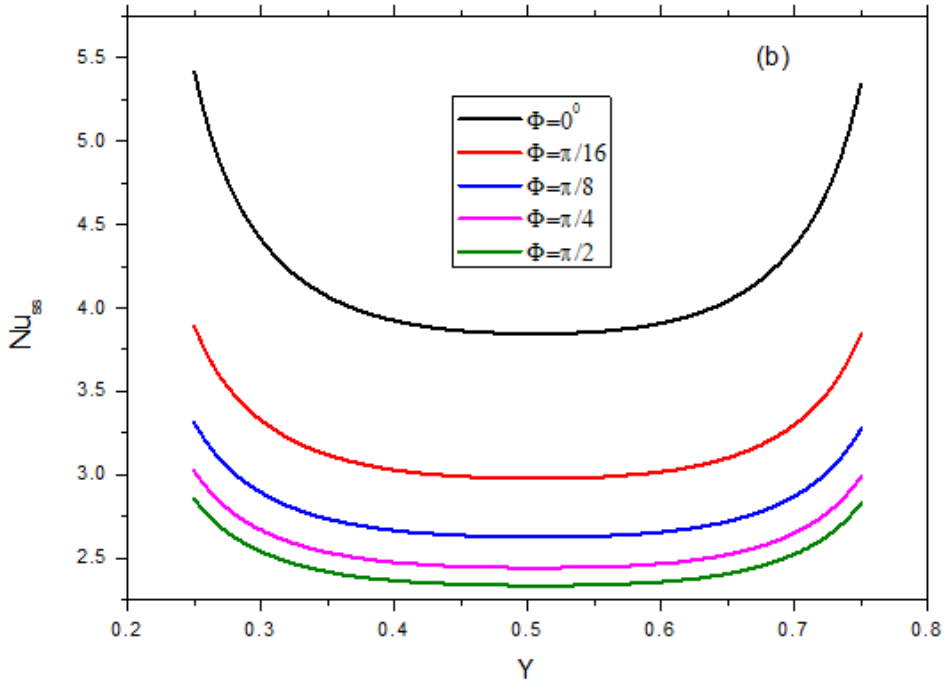
(b)
Φ=0⁰
Φ=π/16
Φ=π/8
Φ=π/4
Φ=π/2
Nu_∞
Y
5.5
5.0
4.5
4.0
3.5
3.0
2.5
0.2
0.3
0.4
0.5
0.6
0.7
0.8

Figure 19